

# Response of Solar-Induced Chlorophyll Fluorescence to Gross Primary Productivity, Evapotranspiration, and Transpiration Under Aridity Gradients of China

Meng Li , Ronghao Chu , Xiuzhu Sha, and Abu Reza Md. Towfiqul Islam 

**Abstract**—The intrinsic relationship between photosynthesis and solar-induced chlorophyll fluorescence (SIF) presents a valuable opportunity for estimating vegetation gross primary productivity (GPP), evapotranspiration (ET), and transpiration (Ec). However, characteristics of the relationship between SIF-GPP, SIF-ET, and SIF-Ec under different regional climatic conditions, such as in various climatic zones, land cover types, and aridity gradients, remain unclear. Thus, the GOSIF and PML\_V2 (China) datasets including GPP, ET, and Ec were employed in the study. We first explored the correlations between SIF-GPP, SIF-ET, and SIF-Ec on annual and monthly time scales across different aridity index (AI). Then, the influence of climatic conditions on correlation coefficients (CCs) between SIF-GPP, SIF-ET, and SIF-Ec were investigated. Finally, the influences of environmental factors on their relationship were further examined. Results showed that SIF, GPP, ET, and Ec all increase as AI increases, with GPP exhibited the most similar variation trends to SIF in both spatial and temporal scales. For the annual time scale, the CC between SIF-GPP, SIF-Ec, and SIF-ET presented similar spatial distribution. Peak correlation values were all occurred in semiarid region (AI is around 0.4). The relationship between SIF-GPP in different climatic zones is generally linear and demonstrated a significant correlation. For monthly time scale, the positive and high CC between SIF-GPP, SIF-Ec, and SIF-ET exhibited obvious “south-north-south” swing trend with increasing AI, with the characteristics of SIF-Ec most consistent with that of SIF-GPP. The relationships between SIF-GPP and SIF-Ec are

Received 24 August 2024; revised 9 March 2025 and 3 May 2025; accepted 19 May 2025. Date of publication 22 May 2025; date of current version 6 June 2025. This work was supported in part by the National Natural Science Foundation of China under Grant 42305207 and Grant 41905100, in part by the Henan Provincial Science and Technology Research Project under Grant 252102321001, in part by the Natural Science Foundation of Henan Province under Grant 252300420300, in part by the Open Foundation of CMA Henan Key Laboratory of Agrometeorological Support and Applied Technique under Grant AMF202403, in part by the Henan Provincial Joint Fund for Science and Technology Research and Development Programs under Grant 242103810091, and in part by Open Fund of Henan General Aviation Technology Key Laboratory under Grant ZHKF-240208. (*Meng Li and Ronghao Chu contributed equally to this work.*) (*Corresponding author: Ronghao Chu.*)

Meng Li is with the School of Civil Aviation, Zhengzhou University of Aeronautics, Zhengzhou 450046, China (e-mail: limeng@zua.edu.cn).

Ronghao Chu is with the China Meteorological Administration, Henan Key Laboratory of Agrometeorological Support and Applied Technique and the Henan Institute of Meteorological Sciences, Zhengzhou 450003, China (e-mail: ronghao\_chu@163.com).

Xiuzhu Sha is with the China Meteorological Administration, Henan Key Laboratory of Agrometeorological Support and Applied Technique and the Weather Modification Center of Henan Province, Zhengzhou 450000, China (e-mail: xiuzhu1990@163.com).

Abu Reza Md. Towfiqul Islam is with the Department of Disaster Management, Begum Rokeya University, Rangpur 5400, Bangladesh, and also with the Department of Earth and Environmental Science, College of Science, Korea University, Seoul 02841, Republic of Korea (e-mail: towfiq\_dm@brur.ac.bd).

Digital Object Identifier 10.1109/JSTARS.2025.3572758

linear, but that between SIF-ET is polynomial nonlinear. We also argued that environmental factors should be considered when using SIF to estimate GPP, ET, and Ec. Results of this study will provide a new reference and possibility for estimating vegetation GPP, Ec, and ET on the monthly and annual scales from large regional scales.

**Index Terms**—Aridity gradients, evapotranspiration (ET), gross primary productivity (GPP), solar-induced chlorophyll fluorescence (SIF), transpiration (Ec).

## I. INTRODUCTION

TERRESTRIAL evapotranspiration (ET) is an essential part of the surface hydrological cycle and plays a crucial role in the water, energy, and carbon cycles [1]. ET is the main way for land water to return to the atmosphere (equivalent to about two-thirds of land precipitation), and it returns up to 60% of the precipitation to the atmosphere, which greatly regulates the surface energy balance [2]. It is primarily composed of transpiration (Ec) from vegetation and evaporation from soil and canopy interception. Among these, vegetation Ec is closely linked to the ecosystem’s carbon cycle process and is crucial in regulating the climate system [3], [4]. Knowing the exact amount of ET in the world’s land and air helps us better understand how the two interact. It is also crucial for figuring out how much water is being used [5], monitoring and predicting droughts [6], and managing water resources in agriculture. This has become one of the most critical topics in global change research in the last decades [7].

With the development of satellite remote sensing, people can retrieve spatially continuous variables such as soil moisture content, vegetation cover and land surface temperature, making large-scale ET estimation possible. In recent decades, a variety of remote sensing-based methods have been developed to estimate ET at different spatial scales [1], [8], [9]. Empirical/semi-empirical models typically combine ground measured ET with remote sensing vegetation parameters such as the vegetation index (VI). Remote sensing models based on meteorological data usually adopt physical models of ET, such as the equation of Penman-Monteith (P-M) or Priestley-Taylor [10], [11]. However, the high nonlinear and lagging relationship between ET and meteorological variables brings some uncertainty to the ET estimation model based on meteorological data [12]. In addition, since water vapor flux and carbon assimilation share a common path, carbon-water coupling methods have also been employed to estimate ET. However, due to the challenge of capturing

vegetation photosynthesis at spatial scales, this approach still has a high uncertainty [13]. Moreover, existing findings also indicate that some challenges still exist in estimating ET at large regional scales.

In terrestrial ecosystems, the processes of photosynthetic activity and nonphotochemical quenching consume photosynthetically active radiation (APAR) that plants absorb, and chlorophyll molecules re-emit the unused APAR in the 400–700 nm spectral range at longer wavelengths. This re-emitted energy is often called solar-induced chlorophyll fluorescence (SIF). SIF can directly show how plant photosynthesis changes over time and is thought to be a direct probe of photosynthesis. It can fix the problems with old optical remote sensing methods, such as using a “greenness” index to measure vegetation, and offer a new way to monitor plant photosynthesis on large scales [14], [15], [16], [17]. Global satellite SIF datasets have been successfully retrieved from the satellite-borne sensors (e.g., SCIAMACHY, GOME-2, GOSAT, TanSat, OCO-2, TROPOMI, and others). The data provided the possibility to study plant photosynthesis on a large regional scale and also provided a new data source for monitoring vegetation growth and environmental stress [18].

Currently, most studies have focused on the strong linear relationship between SIF and gross primary productivity (GPP). The slope of this relationship varies with changes in vegetation coverage, leaf characteristics and canopy structure, vegetation physiological state, and environment elements [19], [20], [21]. Since SIF-GPP is closely related, some studies directly estimate GPP based on SIF using this linear regression methods [22], [23], [24], [25], [26] or include and use SIF data in the GPP modeling framework [27], [28]. The natural coupling of plant Ec and photosynthesis couples canopy Ec with carbon assimilation through stomatal conductance (Gs) at the canopy scale. This essential principal links canopy Ec to VIs and is also the foundation for the above-coupled carbon and water ET method. However, reflectance-based VIs, as representative of satellite optical methods, is not directly linked to the actual photosynthesis process. As a direct substitute for photosynthesis, SIF is expected to improve the estimation of canopy Ec, especially by limiting Gs. Recent advances in exploring SIF provide new opportunities to observe photosynthetic activity from space [22], [24]. Therefore, the development of remote sensing SIF provides the possibility to reevaluate the estimation of large-scale Ec [17], [29], [30], [31], [32].

Considering the coupling between SIF-GPP, some investigations have established a close connection between SIF and Ec or ET. Through flux tower observation data, Lu et al. [33] found a close relationship between SIF and latent heat (LE) flux in temperate forests, and photosynthetically active radiation, vapor pressure deficit (VPD), and air temperature (Tem) are the main influencing factors. Shan et al. [29] observed a strong correlation between SIF-T and SIF-Gs at hourly and daily time scales in forest, farmland, and grassland measurements. At the same time, Shan et al. [30] also attempted to calculate Gs using SIF as an input to the P-M model. They discovered that SIF was an excellent way to measure the conductivity of vegetation canopy and Ec at daily and seasonal levels. Pagán et al. [34] also revealed a strong link between the GOME-2 SIF and the ratio of

Ec to potential evapotranspiration (PET). Moreover, Wang et al. [35] simulate reference crop evapotranspiration ( $ET_0$ ) well using satellite SIF and VPD<sup>0.5</sup>.

Existing studies have only explored the responses of vegetation net ecosystem productivity [36] or vegetation photosynthesis [37], [38] to drought from a unilateral perspective under the aridity gradients, no studies have systematically explored the evolution characteristics of the connection between SIF and GPP (ET or Ec) on a regional scale under different climatic conditions. However, with the intensification of global warming, frequent drought events will have a significant impact on the carbon cycle of terrestrial ecosystems and ET of vegetation [39]. Exploring the relationship among SIF-GPP, SIF-ET, and SIF-Ec under aridity gradients will provide a theoretical basis and reference for estimating GPP, ET, and Ec using SIF under different climatic conditions. Therefore, SIF, ecosystem ET, Ec, and GPP, land use type and meteorological datasets from satellite and meteorological observations are selected in this study, with the primary purposes are as follows.

- 1) To investigate the differences in spatio-temporal evolution characteristics of SIF, GPP, ET, and Ec, as well as the correlations between SIF-GPP, SIF-ET, and SIF-Ec on annual and monthly time scales and their changing trends with AI.
- 2) To explore under what climatic conditions the correlation coefficients (CCs) between SIF-GPP, SIF-ET, and SIF-Ec is highest.
- 3) To reveal the influence of environmental factors on SIF-GPP, SIF-ET, and SIF-Ec relationships. Results of this research will help to fully understand the internal relationship between plant Ec, ET, and photosynthesis, as well as provide a new technique and method for estimating vegetation Ec or ET by SIF from the perspective of remote sensing.

## II. MATERIALS AND METHODS

### A. Weather Data

Here, the datasets of mean temperature (Tem, °C), precipitation (Pre, mm), and sunshine duration (SD, h) at daily time scale from 2416 national meteorological observation stations of China during 2000–2021, were employed to calculate aridity index (AI) and net radiation (Rn, MJ·m<sup>-2</sup>·d<sup>-1</sup>) [see Fig. 1(a)]. These datasets were provided by the China Meteorological Administration<sup>1</sup> and were of good quality control to meet the requirements of this research. Due to the lack of Rn observation data, the Angstrom formula was employed to estimate daily Rn based on SD data. Detailed calculation process can be referred to our previous study [40].

### B. Satellite SIF

In this study, considering the spatiotemporal resolution problem of the existing satellite SIF products, the OCO-2 based global SIF dataset (GOSIF, W·m<sup>-2</sup>·μm<sup>-1</sup>·sr<sup>-1</sup>) developed by Li

<sup>1</sup>[Online]. Available at: <http://data.cma.cn/>.

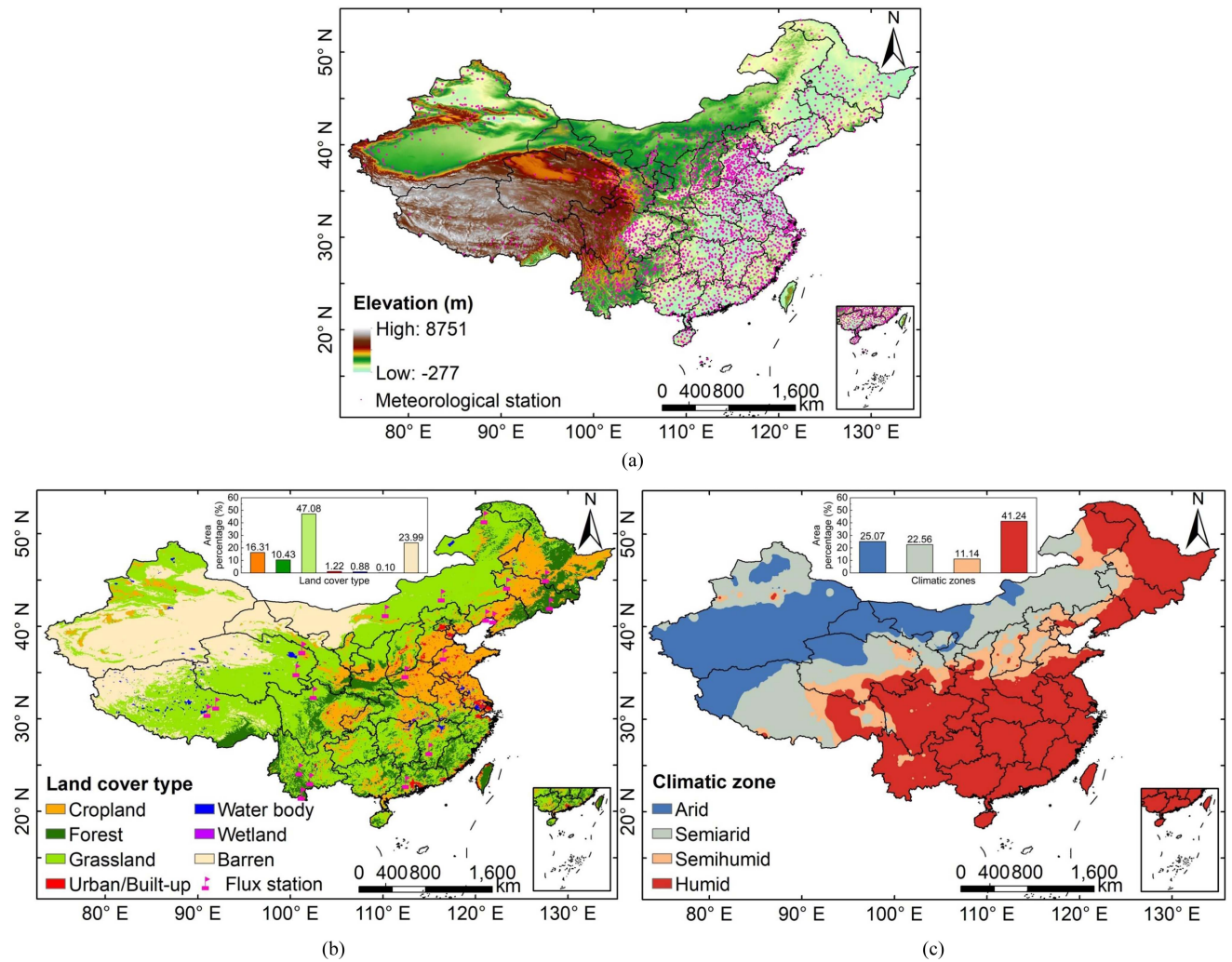


Fig. 1. Spatial characteristics of (a) elevation, (b) land cover type, and (c) climatic zone in China.

and Xiao [23] was employed to explore the changing trends of SIF and the relationship between SIF-GPP, SIF-ET, and SIF-T across aridity gradients. The GOSIF dataset with high spatial ( $0.05^{\circ}$ ) and temporal (8 day, monthly, and annual) resolutions, has a long-time record of continuous global coverage from 2000 to 2024. The performance of this dataset has been validated worldwide by FLUXNET GPP and can be used to assess photosynthesis in terrestrial ecosystems.<sup>2</sup>

#### C. PML\_V2 (China) Dataset

To investigate the relationship between SIF-GPP, SIF-ET, and SIF-T, the PML\_V2 (China) dataset, equipped with the temporal resolution of daily and the spatial resolution of 500 m and the time span from 26 Feb. 2000 to 31 Dec. 2020 were adopted here. This dataset including GPP, vegetation Ec, and soil evaporation (Es), then the ET can be obtained by adding Ec and Es. Compared to the global version (with a spatiotemporal resolution of 8 days and  $0.05^{\circ}$ , covering the period from Jul. 2002 to Aug. 2019), the

simulation accuracy of PML\_V2 (China) has been significantly improved [41], [42]. Specific improvements and innovations can be referred Online.<sup>3</sup> To match the  $0.05^{\circ}$  GOSIF data accuracy, the GPP, Ec, and ET data in PML-V2 (China) were aggregated and resampled to 8 days and  $0.05^{\circ}$  spatio-temporal resolution to explore the correlation relationships between SIF-GPP, SIF-Ec, and SIF-ET.

#### D. Aridity Index

The AI was used as an indicator of climate dryness in China from 2000 to 2021, which was calculated from the ratio of mean annual Pre to mean annual PET. In this study, the AI used an aridity category of the United Nations Environmental Programme (UNEP). Detailed classification levels have been displayed in Table I. Furthermore, we also adopted the reclassify tool in the ArcMap 10.7 environment to generate the AI category. Specific procedure can be referred to Xu et al. [37] and Xu et al. [38].

<sup>2</sup>[Online]. Available at: [http://data.globalecology.unh.edu/data/GOSIF\\_v2/](http://data.globalecology.unh.edu/data/GOSIF_v2/).

<sup>3</sup>[Online]. Available at: <https://data.tpdc.ac.cn/>.

TABLE I  
CLASSIFICATION LEVELS OF AI

Drought category	Arid	Semiarid	Subhumid	Humid
AI interval	AI≤0.2	0.2<AI≤0.5	0.5<AI≤0.65	AI>0.65

#### E. Ancillary Data

To match the spatiotemporal resolution of GOSIF data, the land cover type (LC) dataset (MCD12C1) from MODIS product (Collection 6),<sup>4</sup> with a period from 2001 to 2020 and a spatial resolution of 0.05°, was employed in this research. This product divided the global LC into 17 categories using the International Geosphere-Biosphere Programme classification. Considering the vegetation types in China, we reclassified the LC into seven categories, namely cropland, forest, grassland, urban/built-up land, water bodies, wetlands, and barren, respectively. Moreover, the effect of abiotic factors on the relationships of SIF-GPP, SIF-ET, and SIF-Ec were investigated by MODIS leaf area index (LAI) product MCD15A2H with 500 m spatial resolution and 8-day temporal granularity from 2003 to 2020, was also used to explore. This product was resampled and aggregated to a 0.05° and monthly scale to match the resolution of the GOSIF data.

China Flux Observation Research Network (ChinaFLUX)<sup>5</sup> provides 20th anniversary thematic dataset, including monthly, daily, and 30-minute flux observations, as well as 30-min routine meteorological data collected from 24 ecological stations [see Fig. 1(b)] between 2003 and 2020 (see Table II).<sup>6</sup> The flux data including net ecosystem exchange (NEE), total ecosystem respiration, gross ecosystem exchange, LE, sensible heat (Hs), and the meteorological data are temperature, radiation, precipitation, and others. The monthly ChinaFLUX GPP data are employed to verify the validity of GOSIF data in China, specific calculation formula is as follows:

$$GPP_{\text{month}} = -NEE_{\text{month}} + R_{e \text{ month}} \quad (1)$$

where the  $GPP_{\text{month}}$ ,  $NEE_{\text{month}}$ , and  $R_{e \text{ month}}$  represent the monthly cumulative value ( $\text{gC} \cdot \text{m}^{-2} \cdot \text{month}^{-1}$ ).

In this study, we also further verified the performance of GOSIF by adopting the GPP dataset in ChinaFLUX station. Fig. 2 depicted good linear relationships between GOSIF-GPP at all sites, and all passed 0.05 level significance test. This phenomenon indicated that the quality of GOSIF data is good and can be effectively used to explore the relationship with ET or Ec.

#### F. Trend Analysis

Pearson correlation analysis was used to calculate the CC between two variables (such as the correlation between SIF-GPP, SIF-ET, and SIF-Ec), and a significance level ( $p$ ) of 0.05 was used to test the corresponding significance level between two variables,  $p < 0.05$  indicates a significant correlation, and vice versa [26], [43]. In addition, the spatiotemporal variation trends of SIF, GPP, ET, and Ec, as well as their mean and standard deviation (SD) values per 0.001 AI bin, were compared in this study.

The mean and SD of correlations were also calculated every 0.001 AI bin to reflect changes in vegetation drought sensitivity.

### III. RESULTS

#### A. Spatiotemporal Change Trends of Annual SIF, GPP, ET, and Ec

As shown in Fig. 3, the mean values, slopes and significance of SIF, GPP, ET, and Ec were calculated respectively. The overall spatial distribution trend of the above four variables gradually decreased from southeast to northwest in China, and the mean ranges were  $-0.0402$  to  $0.4317 \text{ W} \cdot \text{m}^{-2} \cdot \mu\text{m}^{-1} \cdot \text{sr}^{-1}$ ,  $0\text{--}7628.41 \text{ gC} \cdot \text{m}^{-2}$ ,  $0\text{--}1516.14 \text{ mm}$  and  $0\text{--}1455.57 \text{ mm}$ , respectively. In addition, the slope ranges of SIF, GPP, ET, and Ec were  $-0.0067$  to  $0.0102 \text{ W} \cdot \text{m}^{-2} \cdot \mu\text{m}^{-1} \cdot \text{sr}^{-1} \cdot \text{a}^{-1}$ ,  $-339.056$  to  $340.138 \text{ gC} \cdot \text{m}^{-2} \cdot \text{a}^{-1}$ ,  $-66.01\text{--}53.40 \text{ mm} \cdot \text{a}^{-1}$ , and  $-64.20$  to  $71.70 \text{ mm} \cdot \text{a}^{-1}$ , respectively. Among them, the spatial difference of the SIF slope was significant, while that of the GPP and Ec slopes was not apparent, but both have good spatial consistency. Moreover, SIF in 90.8% regions exhibited increasing trends, with 64.15% regions reached significant levels. Regions with decreasing trend were mainly distributed in northwestern and southwestern China. Comparing with SIF, GPP showed the most similar significance trend, followed by Ec, while ET showed the most significant difference. Meanwhile, the percentage of GPP with an insignificant increasing trend increased (49.06%) and that with a significant increasing trend decreased (38.18%) when compared with the significance of SIF trend, and the areas with a decreasing trend increased especially in southern China. In the Ec significance chart [see Fig. 3(I)], the regions where Ec showed a decreasing trend increased significantly (27.01%), especially in southern and northeastern China. However, in the ET significance chart [see Fig. 3(I)], the regional difference in significance was the most obvious. The areas with nonsignificant increase, significant increase, nonsignificant decrease, and significant decrease of ET were 48.90%, 13.07%, 31.62%, and 6.41%, respectively.

To further explore the change trends of SIF, GPP, ET, and Ec, box plot and temporal change trend of the above four variables in different climate zones and different land use types were calculated in Fig. 4.

In different climatic zones, the spatial distribution of the above four variables generally followed the order: Humid>Semihumid>Semiarid>Arid, and the characteristics of the boxplot in SIF, GPP, and Ec were similar. However, the regional differences in ET in semiarid, semihumid, and humid regions were small. Furthermore, SIF in all climatic zones exhibited increasing trends, especially significant ( $p < 0.05$ ) in humid and arid regions with an increasing trend of  $0.0014 \text{ W} \cdot \text{m}^{-2} \cdot \mu\text{m}^{-1} \cdot \text{sr}^{-1} \cdot \text{a}^{-1}$  and  $2.028 \text{ W} \cdot \text{m}^{-2} \cdot \mu\text{m}^{-1} \cdot \text{sr}^{-1} \cdot \text{a}^{-1}$  respectively. Similar phenomenon could also be detected in the variation trend of GPP and Ec. However, the trends of ET in all climatic zones were not significant ( $p > 0.05$ ).

In various LCs, the spatial difference of boxplot of each variable was not significant, and there is no uniform regularity. Similar temporal change trends could also be verified. The SIF and GPP are all increasing significantly, except for the SIF in wetland and the GPP in barren. Moreover, the change trends of

<sup>4</sup>[Online]. Available at: <https://search.earthdata.nasa.gov/>

<sup>5</sup>[Online]. Available at: <http://www.chinaflux.org/>

<sup>6</sup>[Online]. Available at: <http://www.nesdc.org.cn/>

TABLE II  
DESCRIPTIONS OF CHINAFLUX DATASETS

Station (Abbreviation)	Longitude (°)	Latitude (°)	Altitude (m)	Time period	Vegetation type
Dinghushan (DHS)	112.5344	23.1737	300	2003-2010	Mixed coniferous broad-leaved forest
Haibei1 (HB1)	101.3119	37.6094	3200	2015-2020	Alpine meadow
Haibei2 (HB2)	101.3333	37.6667	3200	2003-2020	Alpine shrubland
Haibei3 (HB3)	101.3167	37.6000	3200	2004-2009	Alpine wetland
Xilinhot (XLHT)	116.4040	43.3255	1250	2003-2010	Temperate desert steppe
Xishuangbanna1 (XSBN1)	101.2500	21.9167	756	2003-2015	Tropical seasonal rain forest
Xishuangbanna2 (XSBN2)	101.2667	21.9000	592	2010-2014	Rubber plantations
Yucheng (YC)	116.6000	36.9500	28	2003-2010	Winter wheat and summer maize
Changbaishan (CBS)	128.0958	42.4025	738	2003-2004	Broad-leaved red pine forest
Dangxiong (DX)	91.0833	30.8500	4333	2004-2010	Alpine meadow
Jinzhou (JZ)	121.2017	41.1481	23	2005-2014	Spring maize
Ailaoshan (ALS)	101.0289	24.5381	2400-2600	2009-2013	Subtropical evergreen broad-leaved forest
Xiaolangdi (XLD)	112.4689	35.0292	410	2016-2017	Quercus variabilis plantation
Sanjiangyuan (SJY)	100.6992	35.2531	3950	2012-2016	Elymus nutans artificial grassland
Yuanjiang (YJ)	102.1775	23.4739	553	2013-2015	Dry-hot valley ecological station
Naqu (NQ)	92.0167	31.6500	4585	2014-2018	Alpine meadow
Huzhong (HZ)	121.0178	51.7811	773	2014-2018	Boreal forest
Damao (DM)	110.3315	41.6440	1409	2015-2018	Temperate desert steppe
Zoige (ZG)	102.5500	32.8000	3500	2015-2020	Alpine meadow
Maoershan (MES)	127.6667	45.4000	/	2016-2018	Deciduous broad-leaved forest
Panjin1 (PJ1)	121.9603	40.9414	2	2018-2020	Paddy fields
Panjin2 (PJ2)	121.9646	40.9327	2	2018-2020	Reed wetlands
Changling (CL)	123.4703	44.5967	143	2018-2020	Alkali-saline paddy rice
Qianyanzhou (QYZ)	115.0667	26.7333	108	2003-2010	Evergreen Needleleaf Forests

ET in wetland and that of Ec in forest and grassland were significant. Thus, the response sensitivity of the above-mentioned four variables to different climate zones is higher than that to different land use types.

Due to the sensitivity of the above-mentioned four variables to different climate zones being larger than that of different land use types, we further analyzed the variation trends of SIF, GPP, ET, and Ec with increasing AI, namely every 0.001 AI bin. From Fig. 5, we may find that the SIF showed a rapid increasing trend with the increasing AI in general, and when the AI increased between 0.4 and 1.0, SIF increased most rapidly; then the growth trend slowed down. When AI exceeded 2.0, the value range included was very small and relatively dispersed, with an overall decline trend. Compared to SIF, GPP and Ec showed similar variation trends in general. The difference is that GPP and Ec have a valley value when the AI value is around 1.5, then GPP and Ec both show a slowly increasing trend. When AI exceeded 2.0, the data sample size was smaller and more dispersed compared to SIF. Furthermore, different from SIF, GPP, and Ec, the ET exhibited a rapid increasing trend when AI is less than 0.7, then the growth trend of ET slows down with the increase of AI, and there are two valleys when AI is about 0.8 and 1.5.

#### B. Spatiotemporal Variation Trends of Monthly SIF, GPP, ET, and Ec

Monthly variations of SIF, GPP, ET, and Ec in different climatic zones were shown in Fig. 6. Generally, SIF, GPP, ET, and Ec all exhibited similar and significant monthly variation characteristics, and the differences between each climate zone

were obvious. However, the peak values of SIF, ET, and Ec occurred in July, while that of the GPP occurred in August. Moreover, the monthly variation trend of ET was significant in the arid region, while that of the SIF, GPP, and Ec is small.

#### C. Spatiotemporal Variation Trends of the SIF-GPP, SIF-ET, and SIF-Ec Relationships at Annual Time Scale

From the above-mentioned analysis, it showed that SIF, GPP, ET, and Ec all have similar characteristics in spatial and temporal, thus we further explored the spatiotemporal correlation relationships between SIF-GPP, SIF-ET, and SIF-Ec during 2000–2020 at an annual time scale. From Fig. 7, the CCs between SIF-GPP, SIF-ET, and SIF-Ec were  $-0.89$  to 1,  $-0.92$  to 0.98, and  $-0.94$  to 1, respectively [see Fig. 7(a), (c), and (e)]. The overall distribution of CC was similar in spatial, with the high and positive values in the north and low and negative values in the south. The positive correlation area of SIF-GPP was generally larger than that of SIF-ET and SIF-Ec. In addition, the SIF-GPP relationship showed a significant positive correlation in about 55.91% of China, followed by SIF-Ec (42.13%) and SIF-ET (32.28%).

Fig. 8 depicted the variation trends of CC between SIF-GPP, SIF-ET, and SIF-Ec with an increasing AI in every 0.001 AI bin. In general, the SIF-GPP, SIF-ET, and SIF-Ec relationship showed a fluctuating variation trend, initially increasing to the peak, then gradually decreasing to a relatively low value, then slightly increasing and gradually decreasing to a stable state. The SIF-GPP, SIF-ET, and SIF-Ec relationship showed scattered

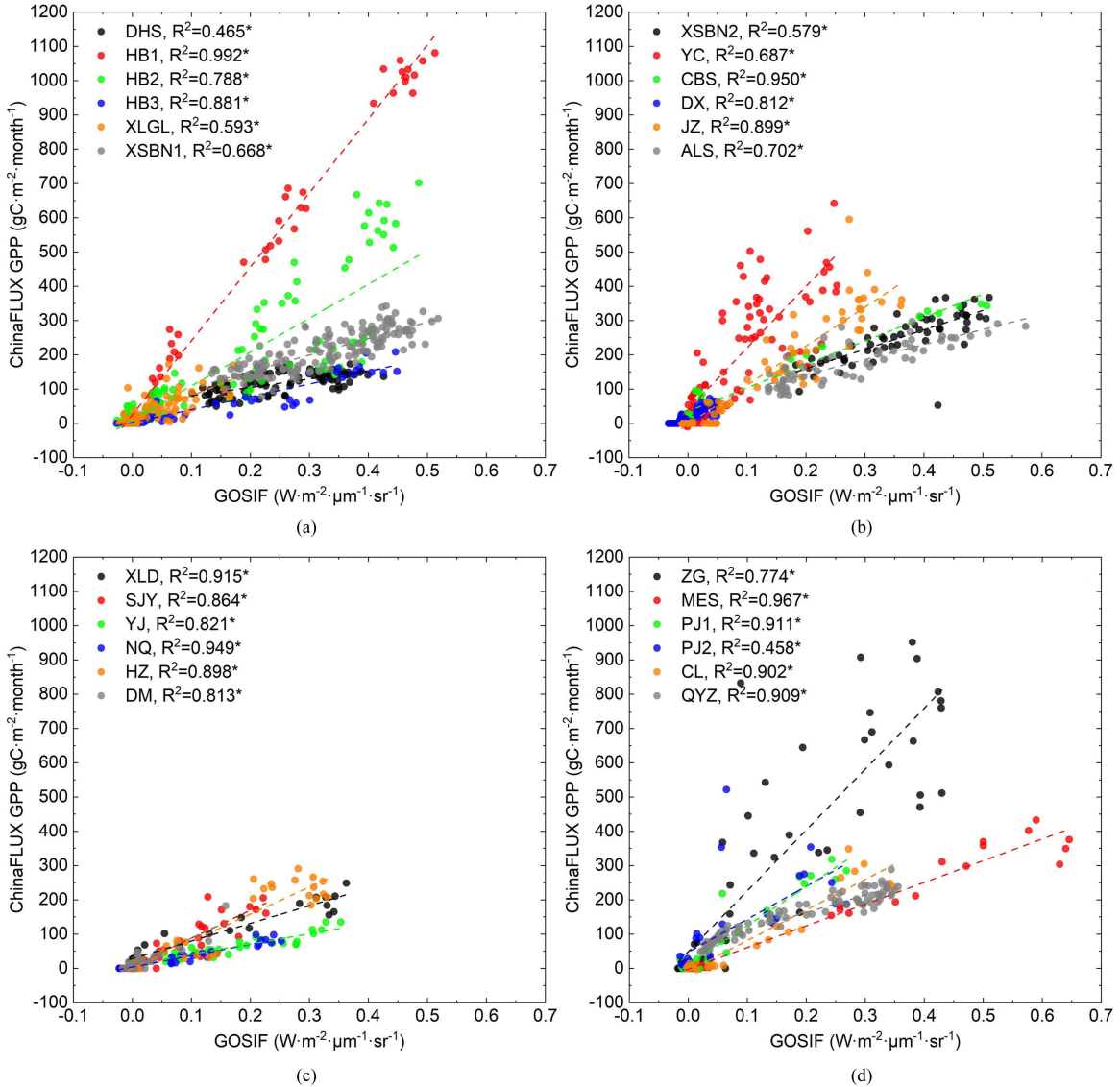


Fig. 2. Scatter fitting between monthly GOSIF and monthly ChinaFLUX GPP at 24 Flux stations of China. Note: Asterisk indicates a significant correlation.

fitting points when the AI exceeded 2.0. The relatively low correlation values all occurred when the AI value was about 0.8. The peak correlation values of SIF-GPP, SIF-ET, and SIF-Ec were 0.74, 0.53, and 0.69, respectively, and they were all occurred when the AI value was around 0.4. Compared to SIF-ET, the variation trends of SIF-GPP and SIF-Ec correlation were more similar, and both showed a downward trend when the AI was less than 0.1.

Furthermore, the SIF-GPP, SIF-ET, and SIF-Ec relationship was investigated on an annual time scale. As shown in Fig. 9, the annual scatter fitting shows that the SIF-GPP relationship is mostly linear and has a strong correlation. The  $R^2$  values for humid, semihumid, semiarid, arid, and the whole regions were 0.90, 0.76, 0.95, 0.90, and 0.98, respectively. However, the CC between SIF-Ec was slightly weaker than that between SIF-GPP, followed by SIF-ET. The  $R^2$  values between SIF-Ec in humid, semihumid, semiarid, arid, and whole regions were 0.34, 0.78, 0.94, 0.84, and 0.99, respectively, and the relationship

in the whole region was polynomial nonlinear. The correlation between SIF-ET revealed a similar nonlinear relationship, with the corresponding  $R^2$  values in humid, semihumid, semiarid, and whole regions were lower than that between SIF-Ec, with values of 0.01, 0.64, 0.38, 0.28, and 0.97, respectively. Except for the humid region, all the relationships showed significant correlation ( $p < 0.05$ ).

#### D. Spatiotemporal Variation Trends of the SIF-GPP, SIF-ET, and SIF-Ec Relationships at Monthly Time Scale

Fig. 10 depicted the spatiotemporal correlation relationships between SIF-GPP, SIF-ET, and SIF-Ec during 2000–2020 at a monthly time scale. The monthly SIF-GPP CC presented significant spatial distribution characteristics and obvious monthly evolution characteristics. Central and southern China primarily distributed the high CC values from January to February. Then, from March to September, the areas with high and positive

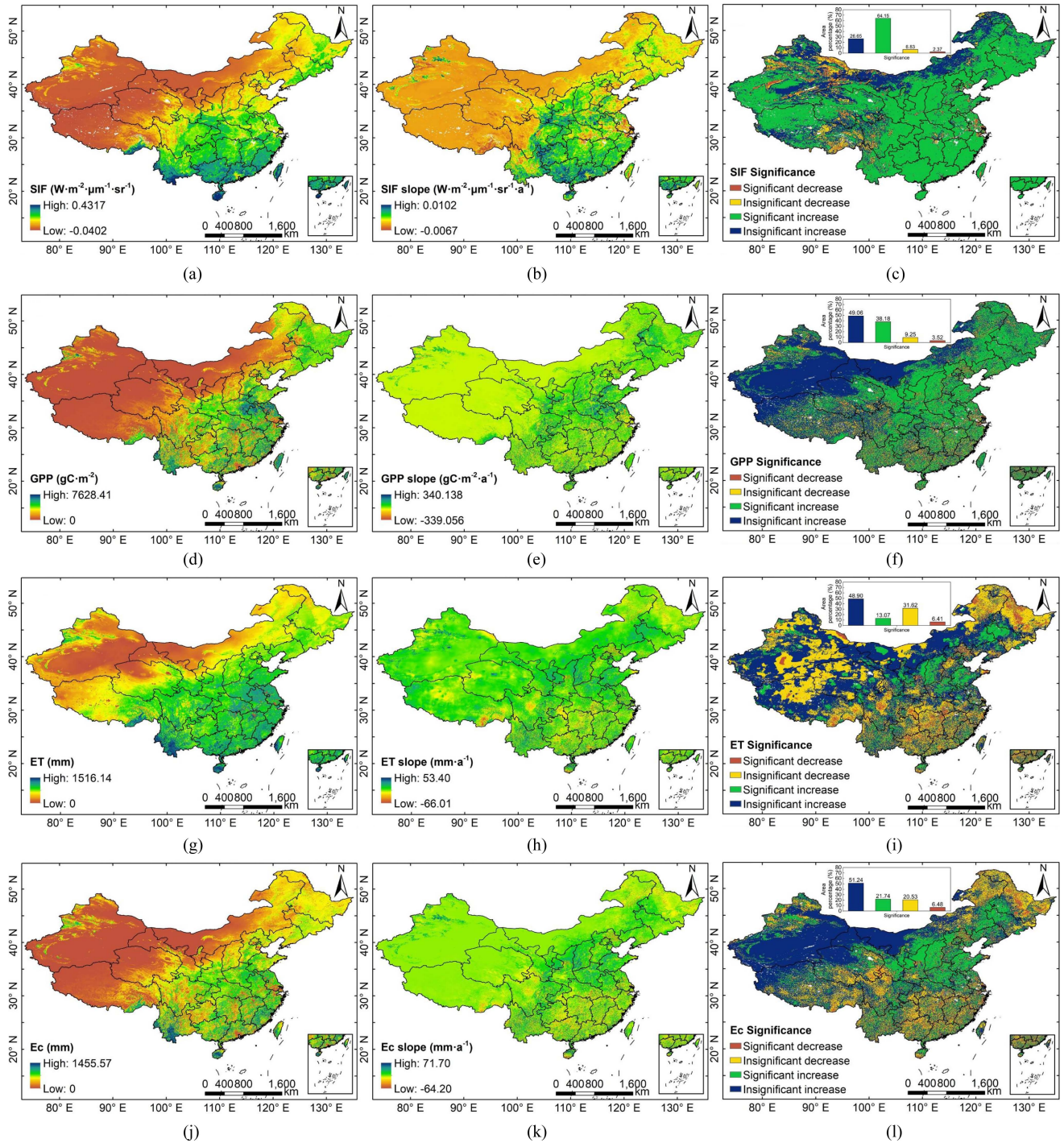


Fig. 3. Spatial characteristics of (a)–(c) SIF, (d)–(f) GPP, (g)–(i) ET, and (j)–(l) Ec values, and their slope and significance in China.

correlation values were gradually shrinking from south to north. However, from October to December, the areas with high and positive correlation values were consisted with those in January and February, gradually shifting to southern China again. The significance between SIF-GPP on the monthly time scale also confirmed this phenomenon. Besides, the CC and significance between SIF-ET, as well as between SIF-Ec, showed similar patterns to the variation trend of SIF-GPP, especially for SIF-Ec (see Figs. 11 and 12).

In addition, the variational trends of CCs between SIF-GPP, SIF-ET, and SIF-Ec were analyzed with an increasing AI during 2001–2020 on a monthly time scale. According to Fig. 13, during January–February, the correlation of SIF-GPP generally decreased before AI was 0.2 (arid region) and then gradually increased. From March to May, the SIF-GPP correlation increased before AI reached 1.0 and then progressively declined. However, from June to October, the variational trends of the SIF-GPP correlation with an increasing AI were similar to those

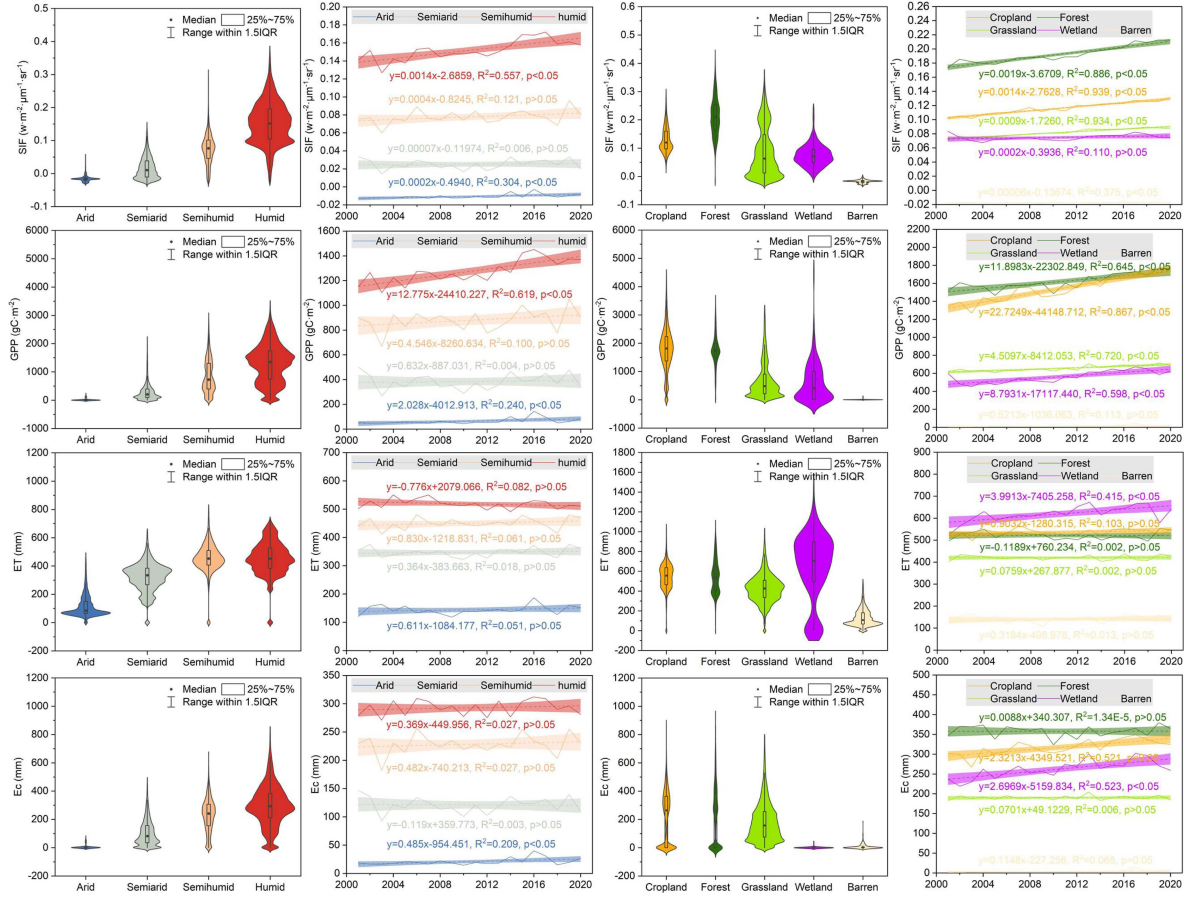


Fig. 4. Box plot and temporal trends of SIF, GPP, ET, and Ec in various climatic zones and land cover types.

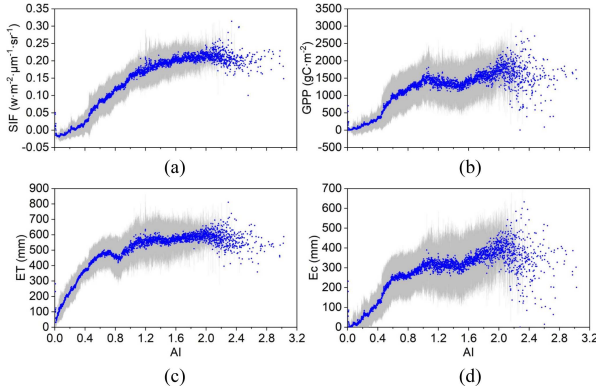


Fig. 5. Variation trends of (a) SIF, (b) GPP, (c) ET, and (d) Ec with increasing AI.

on the annual time scale, generally increasing rapidly before AI reached 0.4 and then gradually decreasing. From November to December, similar to the variation trend in January and February, the SIF-GPP correlation typically showed an increasing trend with the rising AI, especially in December. Moreover, we also found the variation trend of the correlation of SIF-Ec with increasing AI was very close to that of SIF-GPP; thus, we will not describe it in detail here. Although the correlation of SIF-ET also exhibited obvious monthly variation trends, there was somewhat different from that of SIF-GPP and SIF-Ec.

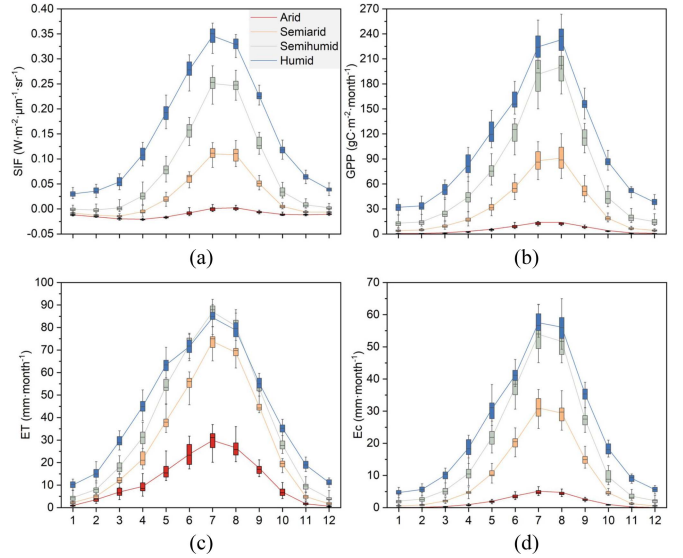


Fig. 6. Box plot of monthly variation characteristics of SIF, GPP, ET, and Ec in various climatic zones.

Given the differences in SIF-GPP, SIF-ET, and SIF-Ec relationships across the increasing AI, we also analyzed the SIF-GPP, SIF-ET, and SIF-Ec relationships on a monthly time scale across different climatic zones. As shown in Fig. 14, SIF and

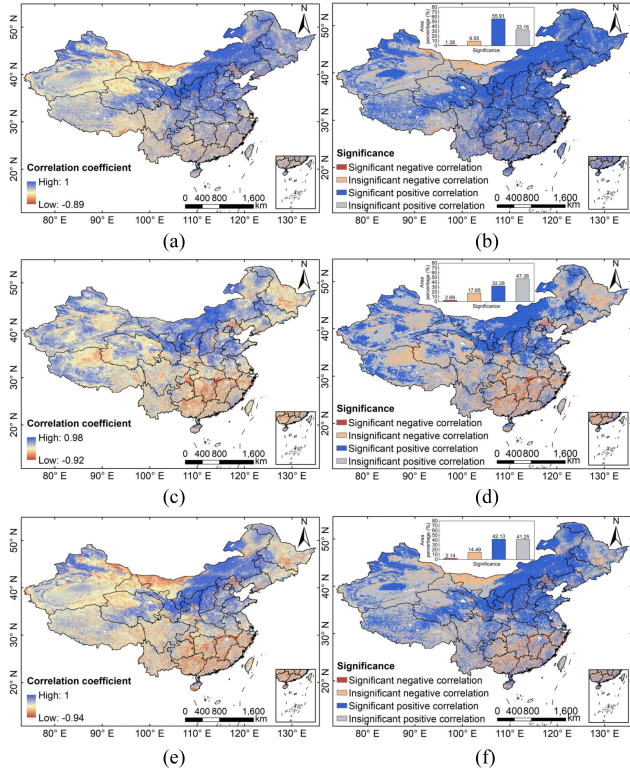


Fig. 7. CC and significance between (a) and (b) SIF-GPP, (c) and (d) SIF-ET, and (e) and (f) SIF-Ec.

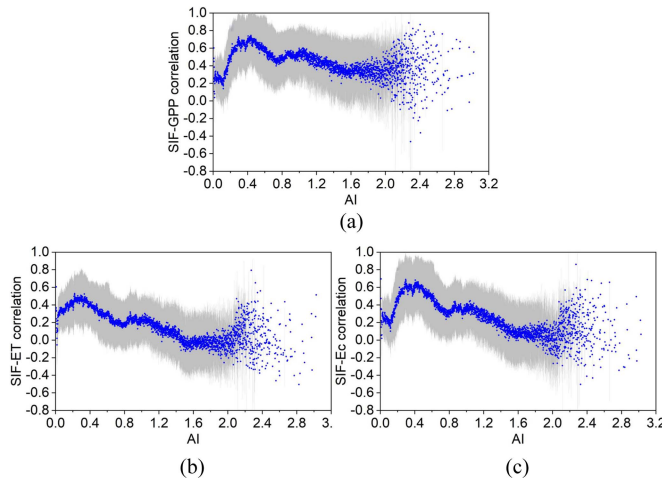


Fig. 8. Variation trends of CCs between (a) SIF-GPP, (b) SIF-ET, and (c) SIF-Ec with increasing AI.

GPP had strong linear relationships on a monthly time scale, with the  $R^2$  values for humid, semi-humid, semi-arid, and arid conditions were 0.97, 0.99, 0.98, and 0.68, respectively. Scatter fitting between SIF-Ec also revealed similar correlation relationships, with the fitting  $R^2$  of 0.98, 0.98, 0.98, and 0.41, respectively. The correlations between SIF-GPP as well as SIF-Ec were significantly lower in arid regions than in others, but all reached the significance level ( $p < 0.05$ ). However, in contrast to the relationships between SIF-GPP and SIF-Ec, SIF-ET demonstrated significant polynomial nonlinear relationships in each

climate region, with the fitting  $R^2$  of 0.94, 0.95, 0.93, and 0.41, respectively. The lower  $R^2$  value in the arid region was consistent with the SIF-GPP and SIF-Ec relationships. Therefore, different climatic conditions will have different impacts on the relationship among SIF-GPP, SIF-ET, and SIF-Ec.

#### E. Influence of Environmental Elements on SIF-GPP, SIF-ET, and SIF-Ec Relationships Under Different Climatic Zones

Sensitivity analysis was employed to reveal the potential influence of environmental elements on the SIF-GPP, SIF-ET, and SIF-Ec relationships under different climatic zones. Using different color bands, Fig. 15 depicted how biotic (LAI) and abiotic (Tem, Pre, Rn, and VPD) drivers affect the SIF-GPP, SIF-ET, and SIF-Ec relationships over a monthly time period. Specifically, Tem, Pre, and LAI appear to cause a covariation with SIF-GPP, SIF-ET, and SIF-Ec in each climatic zone, namely the higher (lower) values the Tem (Pre or LAI) is, the higher (lower) the corresponding SIF, GPP, ET, and Ec will be. However, different from Tem, Pre, and LAI, under the conditions of high Rn and VPD, the corresponding SIF, GPP, ET, and Ec values are not necessarily high, especially for VPD under semihumid, semiarid, and arid conditions. From another perspective, with the synchronous increase of SIF and GPP (ET or Ec), VPD generally showed a changing trend of rising and then falling. The above-mentioned findings indicated that the relationship between the above-mentioned environmental variables and SIF-GPP (SIF-ET and SIF-Ec) can be further considered in the process of using SIF to estimate GPP (ET and Ec), which may effectively improve the overall estimation accuracy.

## IV. DISCUSSION

### A. Relationship Between SIF-GPP, SIF-Ec, and SIF-ET

Satellite observed SIF provides the possibility for Ec observation from large-scale. This is so that canopy conductance can control how much CO<sub>2</sub> photosynthesis takes in and how much water vapor Ec releases [44]. Previous studies [29], [30], [31], [32], [33], [45], [46], [47] have revealed a good relationship between SIF-Ec, but they have not developed the relationship at different time and regional scales. This study thoroughly investigated the relationship between the photosynthetic indicator SIF and the ET and Ec of vegetation in China at the regional scale, thereby providing a new and effective method for better predicting vegetation Ec in spatial contexts.

In this research, we used the correlation relationship between SIF-Ec and SIF-ET to analyze the sensitivity of vegetation photosynthesis to water demand. Results of this study indicated that Ec exhibited better spatiotemporal consistency and correlation with satellite SIF and GPP on both spatiotemporal scales when compared to ET. The sensitivities of SIF to water demand indicators ET and Ec were weaker than those of GPP. This is mainly due to the inclusion of soil evaporation in ET [41], [42], whereas SIF is a direct probe of vegetation photosynthesis and has no correlation with soil information. The negative correlation between SIF-ET and SIF-Ec in southern China (see Fig. 7) can be explained by the decrease in Ec and ET in this region (see Fig. 3).

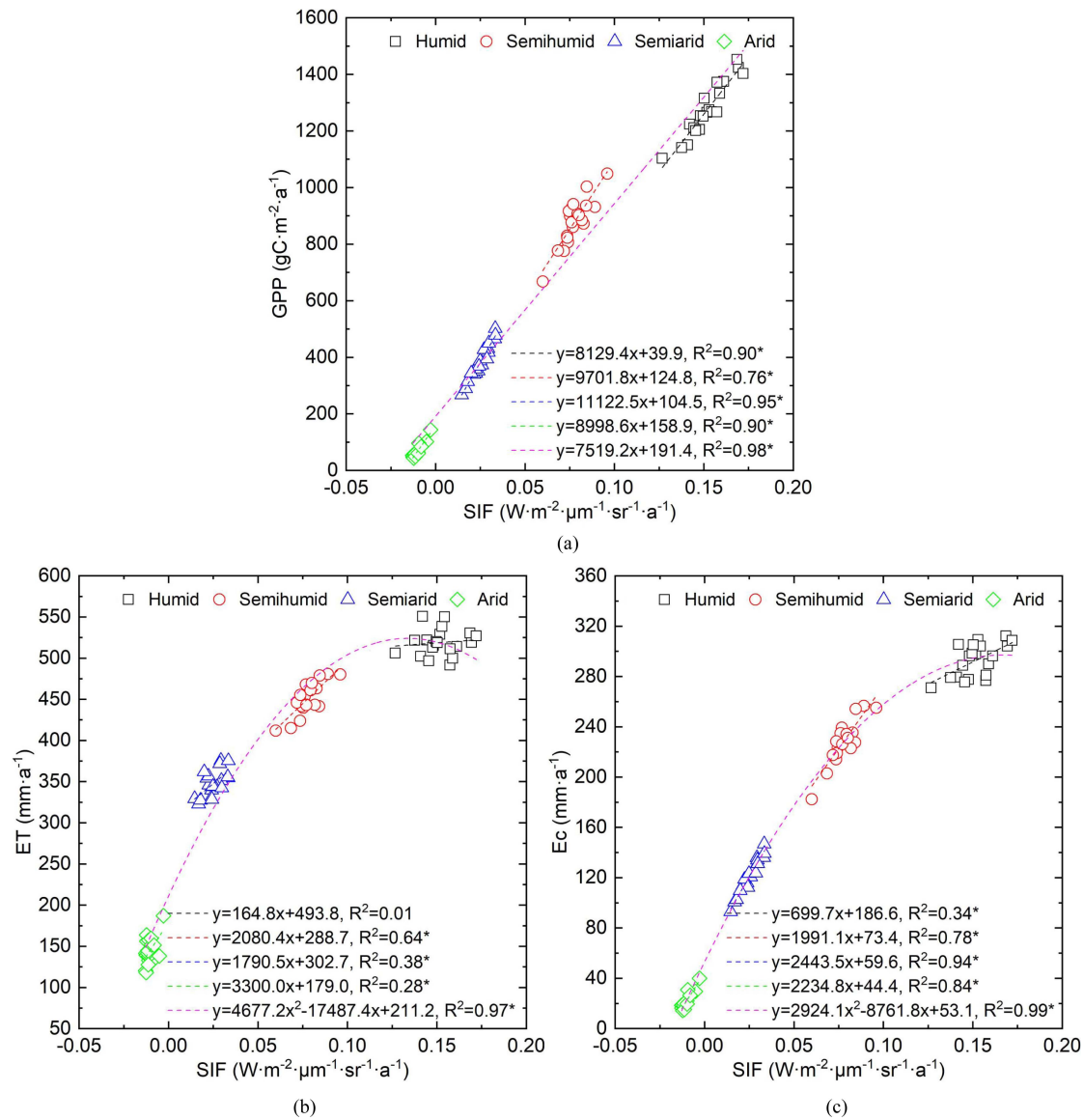


Fig. 9. Scatter fitting between SIF-GPP, SIF-ET, and SIF-Ec at annual time scale.

Due to the combined effects of high VPD and low soil moisture in semiarid areas, regional ecosystems may become more vulnerable in global warming, which could eventually lead to the increased plant mortality and widespread land degradation [48], [49]. In semiarid regions, grassland is the primary vegetation cover type (see Fig. 1). Due to its shallow root depth, the growth of grassland depends heavily on the water content of the surface soil and is sensitive to dynamic precipitation. Therefore, future research should strengthen the influence of water parameters in arid and semiarid ecosystems.

Furthermore, this study evaluated the SIF-GPP, SIF-ET, and SIF-Ec relationship on annual (see Fig. 9) and monthly (see Fig. 14) time scales. The nonlinear relationship was detected in annual SIF-ET and SIF-Ec of China, and the monthly SIF-ET in each climatic zone. When we consider soil evaporation in ET and compared it with Ec, the linear relationship between SIF-Ec transforms into a nonlinear relationship between SIF-ET. Although SIF is not necessarily associated with soil evaporation, the nonlinear relationship between SIF-ET at the monthly scale

in Fig. 14 provides a solid basis for using SIF to estimate ET. Qiu et al. [50] found that varying aridity and different SIF observation times would influence the SIF-GPP relationship. Bai et al. [51] found that the accuracy of SIF-based GPP estimation could be improved by considering the dynamic variation of the GPP/SIF ratio. This study found a good spatiotemporal consistency between GPP and Ec, so the excellent relationship between SIF-GPP could also provide a reasonable theoretical basis for using SIF to estimate Ec on a regional scale.

#### B. Influence of Aridity Gradients on Relationship Between SIF-GPP, SIF-Ec, and SIF-ET

When the AI value exceeds 0.4, the current study could also find a significant downward trend in the CC between SIF-GPP, SIF-ET, and SIF-Ec (see Figs. 7 and 8). Research indicated that abundant precipitation and many forests and croplands in semihumid and incredibly humid regions reduce the water requirements of vegetation, increase water use efficiency, and

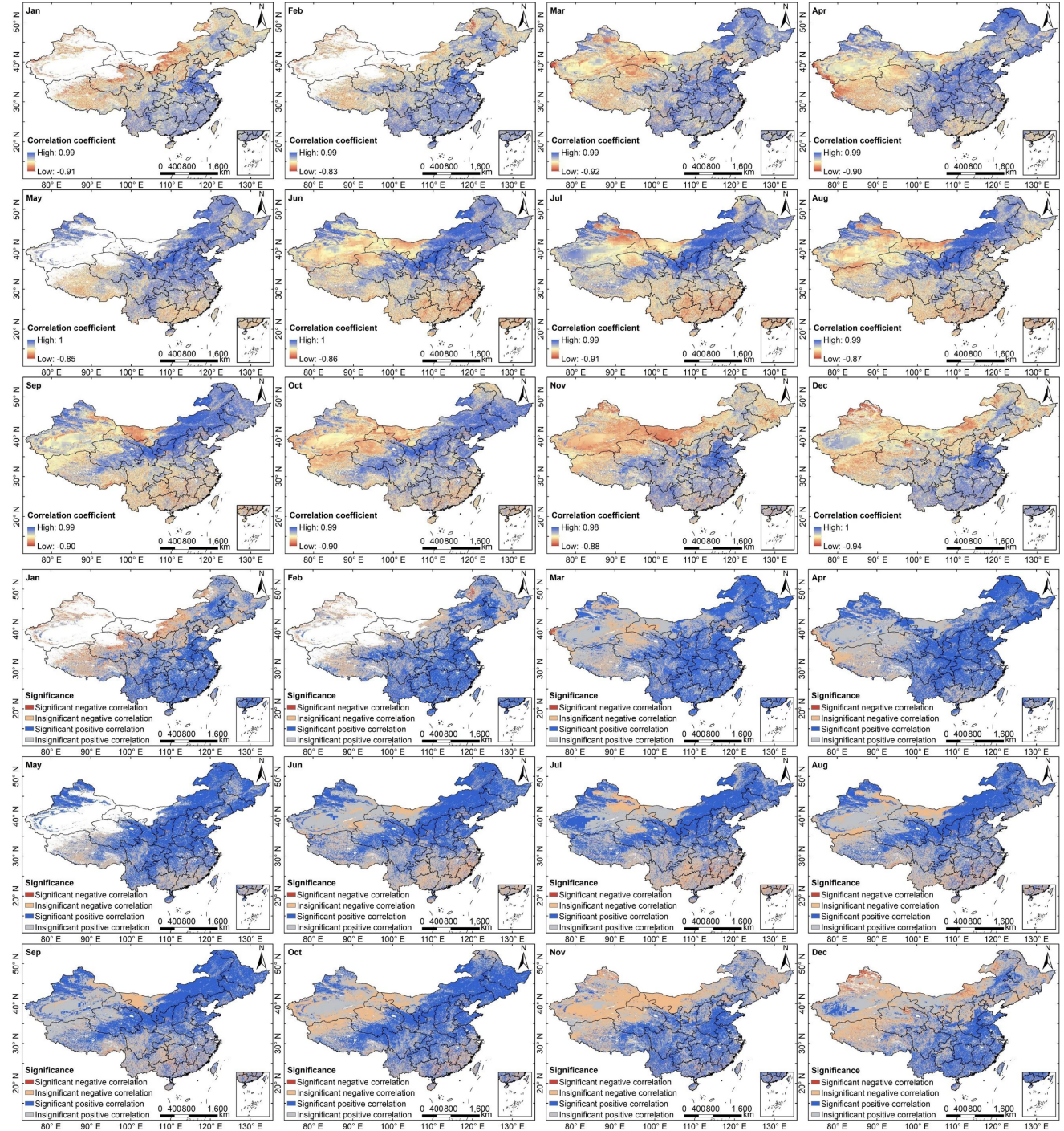


Fig. 10. Correlation relationships between SIF-GPP in monthly time scale.

increase sensitivity to drought [52]. Among them, forests have strong drought resistance due to deep roots, unique water storage systems, and long life, while agricultural management measures such as crop rotation, irrigation, and fertilization can change the response of crop photosynthesis to water demand and drought [53], [54]. Moreover, this study also detected that the CCs between SIF-GPP, SIF-ET, and SIF-Ec all exhibited prominent monthly variation characteristics (see Figs. 10–13). The vegetation's sensitivity, resilience, and vulnerability to climate variability could explain this [55]. This phenomenon deserves further

attention, and the difference in SIF-ET and SIF-Ec relationships in different climatic zones and different monthly time scales, should be considered when using SIF to estimate ET and Ec at a regional scale.

Furthermore, this study discovered that the peak correlation values of SIF-GPP, SIF-ET, and SIF-Ec all appeared around the AI value of 0.4 and the value range belongs to the semiarid region (see Table I). Similar results could also be found in the relationship between SIF and SPEI with increasing AI in the northwestern China [37], [38], the nonlinear parabolic pattern

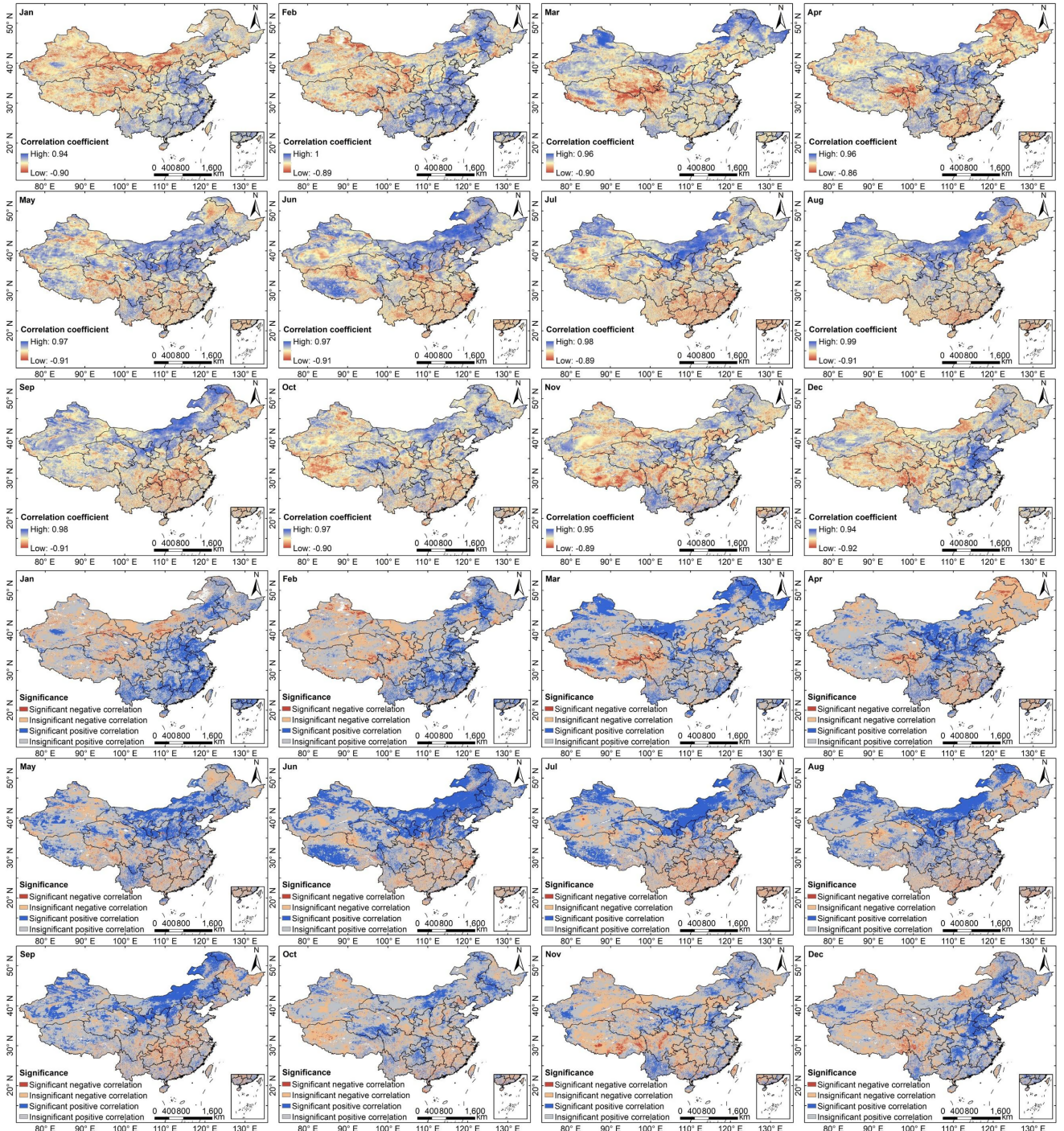


Fig. 11. Correlation relationships between SIF-ET in monthly time scale.

of vegetation sensitivity changes along the aridity gradient in arid and semiarid regions [56], and the highest and most significant nonlinear variations of drought sensitivity of grassland in semiarid zones [57]. Past research has shown that semiarid ecosystems are beneficial for studying how the global NEE changes over time and how it can be unpredictable [58]. Zhan et al. [59] also reported that the vegetation greening rate in southeast arid and semiarid areas of China is higher than in the northwest. Results of this study demonstrate that vegetation photosynthetic probe SIF exhibited an intense and rapid response to vegetation water parameters ET and Ec in semiarid ecosystems;

this phenomenon also indirectly confirmed that SIF can achieve a fast response to drought [14], [16], [43]. Previous studies have also shown that when drought exceeds the threshold of ecosystem tolerance, the responses of the ecosystem to climate change may fluctuate nonlinearly [60], [61].

### C. Influence of Environmental Factors on Relationship Between SIF-GPP, SIF-Ec, and SIF-ET

Damm et al. [62] and Zhang et al. [63] both pointed out that the estimation of ET or Ec requires a dataset including SIF, LAI,

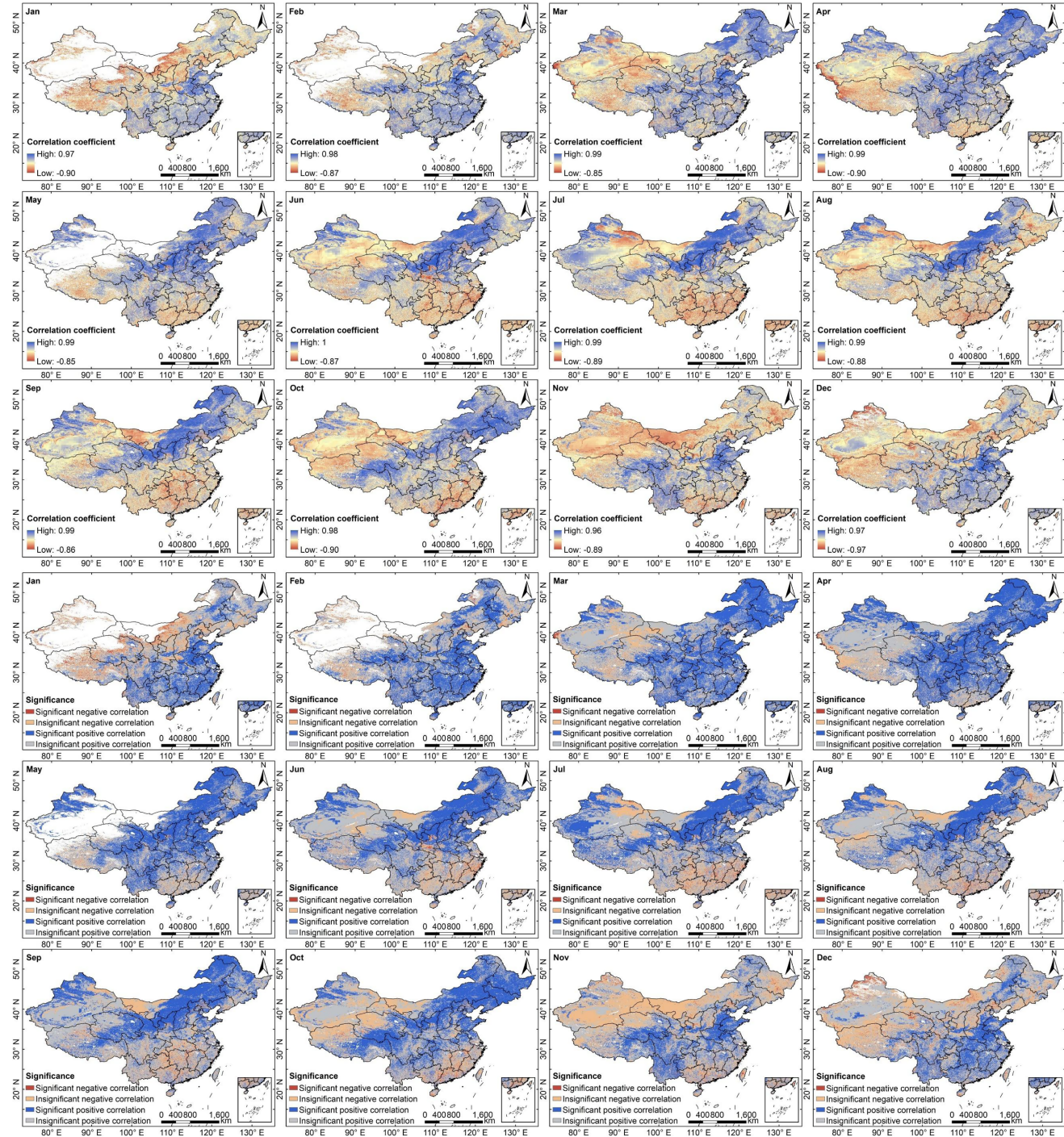


Fig. 12. Correlation relationships between SIF-Ec in monthly time scale.

land use type, and meteorological variables such as Tem, Rad, relative humidity, and so on. Our study found that Tem, Pre, and LAI were positively associated with SIF-GPP, SIF-ET, and SIF-Ec from the regional monthly time scale. However, VPD and Rn generally increased first and then decreased with the synchronous increase of SIF and GPP (ET or Ec). This finding differed from that of Yang et al. [44], who reported that the VPD plays a leading role in determining dryness stress on Ec across most vegetated areas. Wang and Zhang [64] also verified that the linear SIF-GPP correlation gradually decreases with the increase

of Tem. When Tem is high, the SIF-GPP correlation is weakened in a subtropical evergreen coniferous forest. Furthermore, many studies have also highlighted the importance of VPD when estimating ET and Ec using SIF [30], [33], [35], [44], [45], [65]. However, when environmental conditions exceed a certain threshold or under the extreme environmental conditions, the linear relationship between SIF-Ec and SIF-ET may deteriorate and the SIF may not be a direct substitute parameter for GPP, Ec, and ET [66]. In addition, previous studies also pointed out that the importance of leaf physiology should be emphasized in

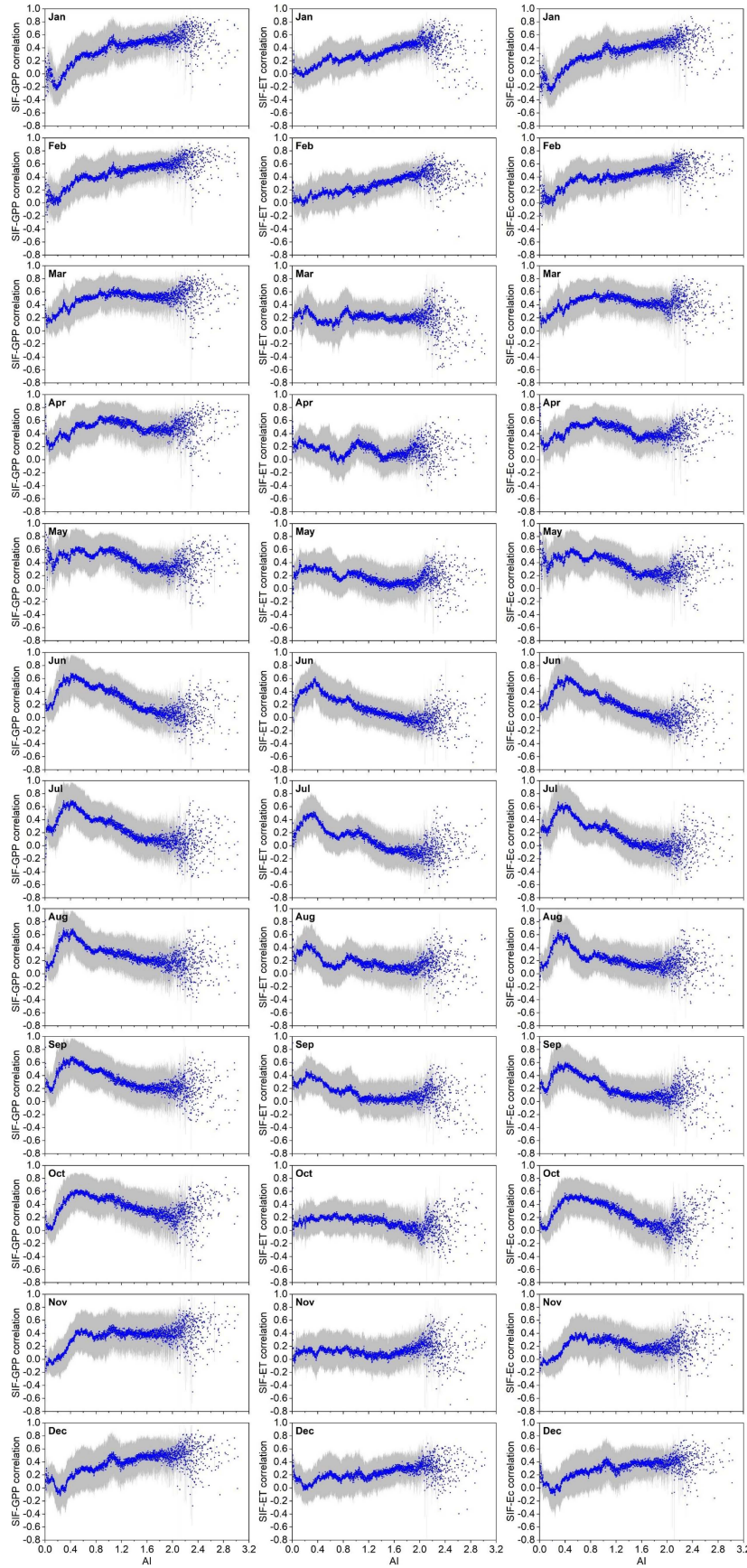


Fig. 13. Variation trends of CCs between SIF-GPP, SIF-ET, and SIF-Ec with increasing AI during 2001–2020 at monthly time scale.

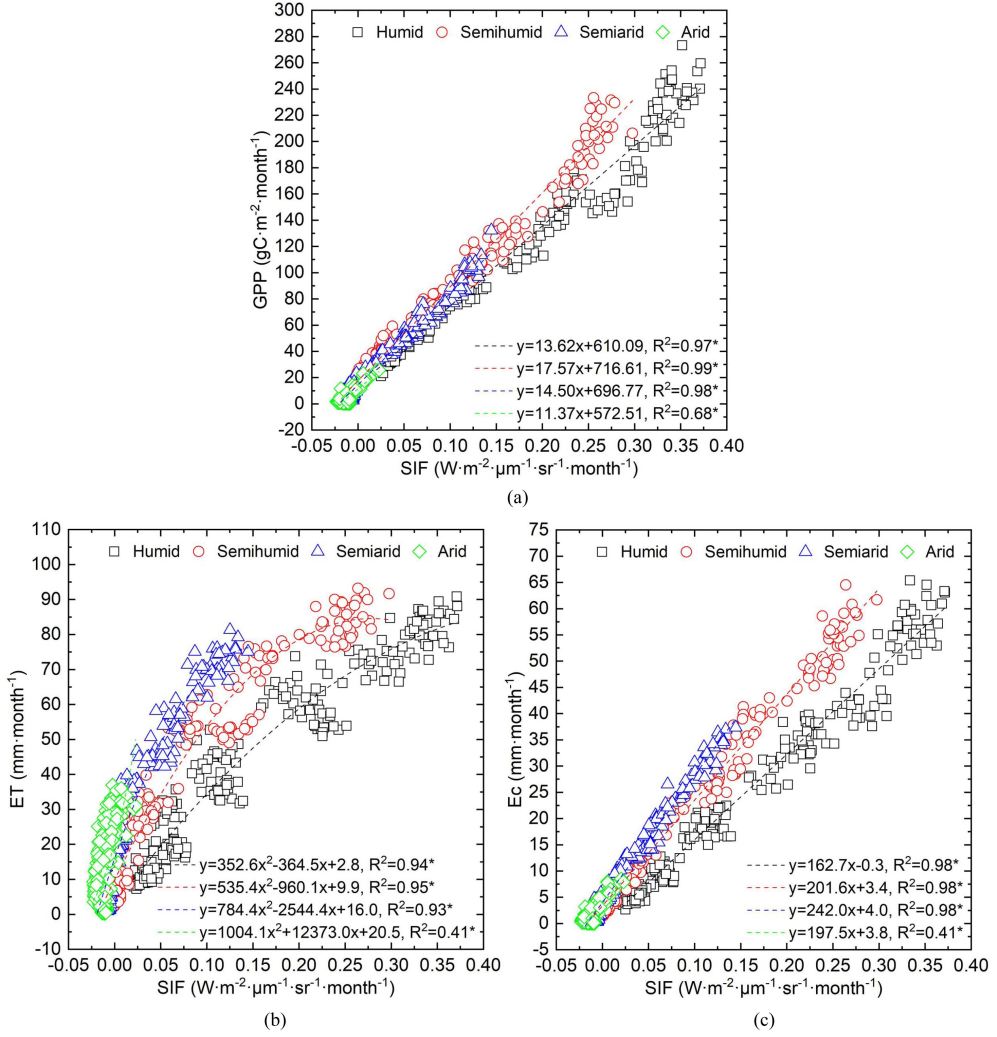


Fig. 14. Scatter fitting between SIF-GPP, SIF-ET, and SIF-Ec in monthly time scale across different climatic zones.

exploring the SIF-GPP relationship in crops, and the introduction of PRI under high VPD conditions can effectively improve the accuracy of Ec estimation by SIF [45], [67].

Therefore, when using SIF to estimate GPP, ET, and Ec, more consideration should be given to the influence of environmental factors and the mechanism of their relationship, to improve the estimation accuracy of ET and Ec in future research.

#### D. Limitations and Future Work

Although some interesting conclusions have been depicted in this research, some shortcomings and limitations still exist in the research process. First, only one data product of SIF (GOSIF) and GPP, Ec, and ET [PML-V2 (China)] was employed to explore the relationship between SIF-GPP, SIF-Ec, and SIF-ET in this study, whether there are some different relationships between various SIF products and various GPP, Ec, and ET products, which still needs further research. Second, although the performance of GOSIF has been verified by ChinaFLUX observed GPP data from 24 Flux stations, more available ChinaFLUX measured GPP data and ChinaSpec measured SIF data

can be used in future to further verify GOSIF and other SIF products. Furthermore, the GOSIF data was reconstructed from the OCO-2 SIF data and its spatial resolution was improved to  $0.05^\circ$  [23], the accuracy was still relatively rough and could not match the 500-m spatial resolution accuracy of the PML-V2 data. Therefore, there may be some uncertainty when exploring the relationship between SIF-GPP, SIF-Ec, and SIF-ET. Although the PML\_V2 dataset provided sufficiently accurate estimates of GPP, ET, and Ec with higher spatial and temporal resolution, it was calculated through multiple meteorological and remote sensing data by employing a complex machine learning model. Since SIF is a direct probe of photosynthesis, exploring its relationship with GPP, ET, and Ec will provide more convenient and effective methods and technical means for the estimation of GPP, ET, and Ec. Presently, there are no satellite sensors specifically designed for detecting SIF at present, the SIF data inverted by satellites still have problems such as low spatial resolution, discontinuous spatial sampling and short time series. Subsequent research will focus on reconstructing higher-resolution SIF product datasets or hope to utilize the high-resolution SIF data directly observed by the upcoming FLEX

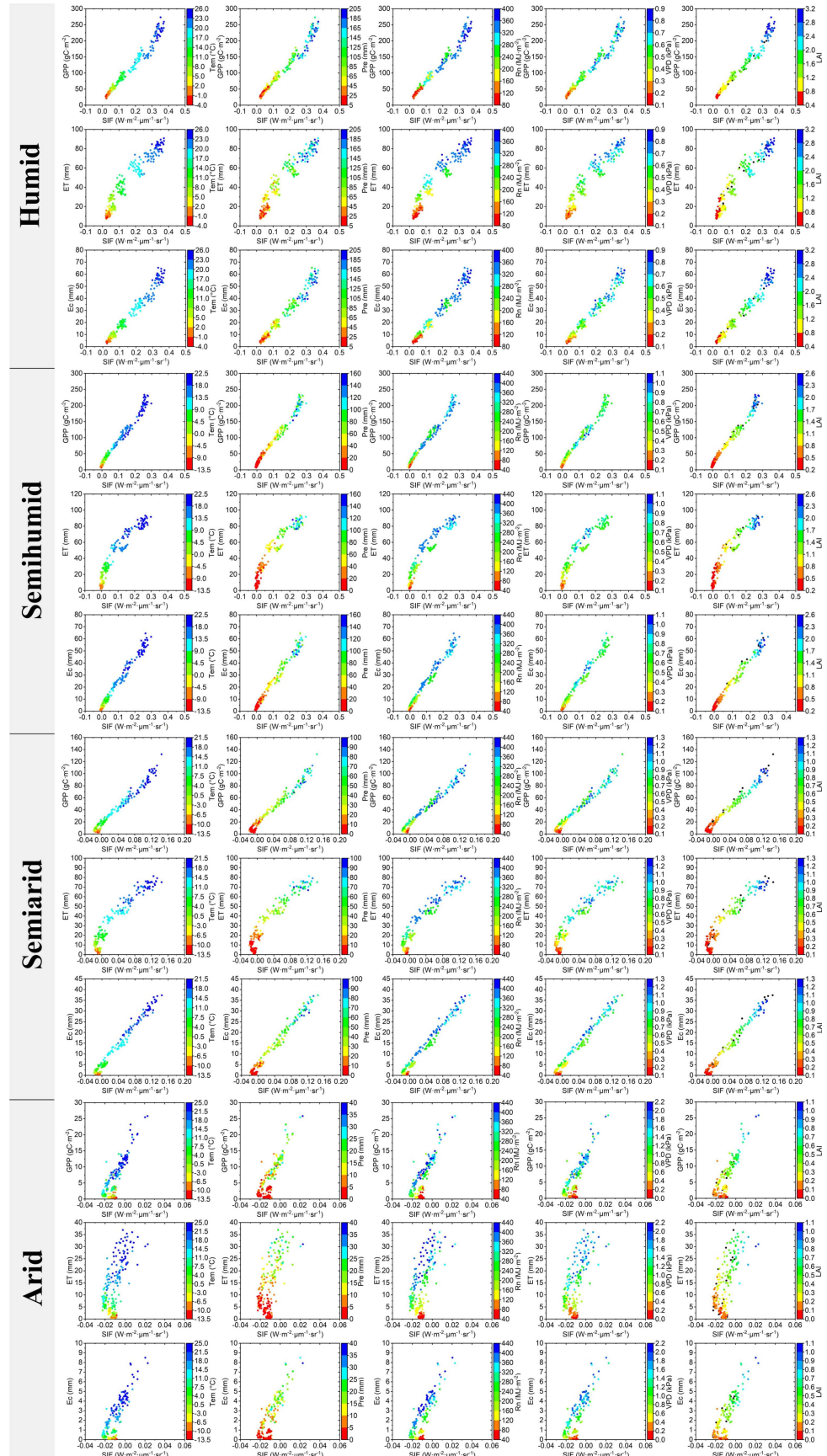


Fig. 15. Relationship between SIF-GPP, SIF-ET, and SIF-Ec under different Tem, Pre, Rn, VPD, and LAI conditions at monthly time scale.

satellite launched by America [17] and the Goumang satellite already launched by China in 2022 [68]. When the accuracy of SIF products is improved, its ability in estimating regional scale GPP, ET and T will be significantly enhanced. Thirdly, although the current study revealed a good relationship between SIF-Ec and SIF-ET from the macroregional scale, future studies still need to focus on the field microscopic scale. Specific tasks can be further explored the relationship between field actual observed SIF and actual Ec and ET of different crop species in the field at half-hour, hourly, daily, monthly, and seasonal scales based on the ChinaFLUX and ChinaSpec network observation data to provide better technical support for accurate estimation of ET and Ec.

## V. CONCLUSION

This study systematically explored the relationship between SIF and GPP, Ec and ET in different climate regions of China on annual and monthly time scales and effectively evaluated the possibility of using SIF to estimate GPP, Ec, and ET on a regional scale. Specific conclusions are as follows.

- 1) Spatial distribution characteristics of SIF, GPP, ET, and Ec all gradually decreased from southeast to northwest, China, with the values follow the order: Humid>Semihumid>Semiarid>Arid. SIF, GPP, ET, and Ec showed a logarithmic increase with increasing AI, with the GPP and Ec are closer to each other. Similar variation trends could also be revealed on a monthly time scale. When the AI value exceeds 0.4, a significant downward trend in the CC between SIF-GPP, SIF-ET, and SIF-Ec was found.
- 2) On annual time scale, the spatial characteristics of the CC between SIF-GPP, SIF-Ec, and SIF-ET were similar, with high and positive values in the north and low and negative values in the south. The SIF-GPP relationship in different climatic zones was generally linear and exhibited a significant correlation, while the SIF-Ec and SIF-ET correlation in the whole region is polynomial nonlinear and slightly weaker than that of SIF-GPP. On a monthly time scale, the SIF-GPP, SIF-ET, and SIF-Ec correlation all displayed a monthly variation characteristic of “South-North-South” swing with increasing AI, and the variation trend of SIF-Ec was most consist with that of SIF-GPP. SIF-GPP and SIF-Ec all showed significant linear correlation relationships in each climate zone, while SIF-ET showed significant polynomial nonlinear relationships.
- 3) Tem, Pre, and LAI appear to covariate with SIF-GPP, SIF-Ec, and SIF-ET, whereas the VPD and Rn generally increased first and then decreased with the synchronous increase of SIF and GPP (ET or Ec). Effects of environmental factors should be considered when using SIF to estimate GPP, ET, and Ec.

## ACKNOWLEDGMENT

The author would like to thank all the scholars, editors, and anonymous reviewers who helped to write and improve this article.

## REFERENCES

- [1] M. Jung et al., “Recent decline in the global land evapotranspiration trend due to limited moisture supply,” *Nature*, vol. 467, pp. 951–954, 2010.
- [2] Q. Zhang et al., “Reforestation and surface cooling in temperate zones: Mechanisms and implications,” *Glob. Change Biol.*, vol. 26, no. 6, pp. 3384–3401, 2020.
- [3] S. P. Good et al., “ $\delta^2\text{H}$  isotopic flux partitioning of evapotranspiration over a grass field following a water pulse and subsequent dry down,” *Water Resour. Res.*, vol. 50, no. 2, pp. 1410–1432, 2014.
- [4] S. Jasechko et al., “Terrestrial water fluxes dominated by transpiration,” *Nature*, vol. 496, pp. 347–350, 2013.
- [5] G. R. Diak et al., “Estimating land surface energy budgets from space – Review and current efforts at the University of Wisconsin-Madison and USDA-ARS,” *Bull. Amer. Meteorological Soc.*, vol. 85, no. 1, pp. 65–78, 2003.
- [6] D. J. McEvoy et al., “Improved seasonal drought forecasts using reference evapotranspiration anomalies,” *Geophysical Res. Lett.*, vol. 43, no. 1, pp. 377–385, 2016.
- [7] X. Lian et al., “Partitioning global land evapotranspiration using CMIP5 models constrained by observations,” *Nat. Climate Change*, vol. 8, pp. 640–646, 2018.
- [8] N. Bhattacharai et al., “An automated multi-model evapotranspiration mapping framework using remotely sensed and reanalysis data,” *Remote Sens. Environ.*, vol. 229, pp. 69–92, 2019.
- [9] M. Li et al., “Characteristics of surface evapotranspiration and its response to climate and land use and land cover in the Huai River Basin of Eastern China,” *Environ. Sci. Pollut. Res.*, vol. 28, pp. 683–699, 2021.
- [10] H. Penman, “Natural evaporation from open water, bare soil, and grass,” *Proc. Roy. Soc. London Ser. A*, vol. 193, no. 1032, pp. 120–146, 1948.
- [11] C. H. B. Priestley and R. Taylor, “On the assessment of surface heat flux and evaporation using large-scale parameters,” *Monthly Weather Rev.*, vol. 100, no. 2, pp. 81–92, 1972.
- [12] Q. Zhang et al., “The hysteretic evapotranspiration-vapor pressure deficit relation,” *J. Geophysical Res.*, vol. 119, no. 2, pp. 125–140, 2014.
- [13] Y. Ryu et al., “Integration of MODIS land and atmosphere products with a coupled-process model to estimate gross primary productivity and evapotranspiration from 1km to global scales,” *Glob. Biogeochemical Cycles*, vol. 25, 2011, Art. no. GB4017.
- [14] J. Peng et al., “Research progress of solar-induced chlorophyll fluorescence inversion and its application in monitoring vegetation environmental stress,” *Jiangsu Agricultural Sci.*, vol. 49, no. 24, pp. 29–40, 2021.
- [15] Z. Sun et al., “Research progress and prospective of global satellite based solar-induced chlorophyll fluorescence products,” *Remote Sens. Technol. Appl.*, vol. 36, no. 5, pp. 1044–1056, 2021.
- [16] L. Wu et al., “Remote sensing of solar-induced chlorophyll fluorescence and its applications in terrestrial ecosystem monitoring,” *Chin. J. Plant Ecol.*, vol. 46, no. 10, pp. 1167–1199, 2022.
- [17] Z. Zhang et al., “Retrieval of sun-induced chlorophyll fluorescence and advancements in carbon cycle application,” *J. Remote Sens.*, vol. 23, no. 1, pp. 37–52, 2019.
- [18] G. H. Mohammed et al., “Remote sensing of solar-induced chlorophyll fluorescence (SIF) in vegetation: 50 years of progress,” *Remote Sens. Environ.*, vol. 231, 2019, Art. no. 111177.
- [19] J. Verrelst et al., “Global sensitivity analysis of the SCOPE model: What drives simulated canopy leaving sun-induced fluorescence?,” *Remote Sens. Environ.*, vol. 166, pp. 8–21, 2015.
- [20] Y. Zhang et al., “Model-based analysis of the relationship between sun-induced chlorophyll fluorescence and gross primary production for remote sensing applications,” *Remote Sens. Environ.*, vol. 187, pp. 145–155, 2016.
- [21] C. Van der Tol et al., “Models of fluorescence and photosynthesis for interpreting measurements of solar-induced chlorophyll fluorescence,” *Biogeosciences*, vol. 119, pp. 2312–2327, 2014.
- [22] L. Guanter et al., “Global and time-resolved monitoring of crop photosynthesis with chlorophyll fluorescence,” *Proc. Nat. Acad. Sci. United States Amer.*, vol. 111, no. 14, pp. E1327–E1333, 2014.
- [23] X. Li and J. Xiao, “A global, 0.05-degree product of solar-induced chlorophyll fluorescence derived from OCO-2, MODIS, and reanalysis data,” *Remote Sens.*, vol. 11, 2019, Art. no. 517.
- [24] Y. Sun et al., “OCO-2 advances photosynthesis observation from space via solar-induced chlorophyll fluorescence,” *Science*, vol. 358, no. 6360, 2017, Art. no. eaam5747.
- [25] Z. Zhang et al., “Reduction of structural impacts and distinction of photosynthetic pathways in a global estimation of GPP from space-borne solar-induced chlorophyll fluorescence,” *Remote Sens. Environ.*, vol. 2040, 2020, Art. no. 111722.

- [26] M. Li et al., "Monitoring 2019 drought and assessing its effects on vegetation using solar-induced chlorophyll fluorescence and vegetation indexes in the middle and lower reaches of Yangtze River, China," *Remote Sens.*, vol. 14, no. 11, 2022, Art. no. 2569.
- [27] C. Bacour et al., "Improving estimates of gross primary productivity by assimilating Solar-induced Fluorescence satellite retrievals in a terrestrial biosphere model using a process-based SIF model," *J. Geophysical Res., Biogeosciences*, vol. 124, pp. 2381–3306, 2019.
- [28] A. J. Norton et al., "Estimating global gross primary productivity using chlorophyll fluorescence and a data assimilation system with the BETHYSCOPE model," *Biogeosciences*, vol. 16, pp. 3069–3093, 2019.
- [29] N. Shan et al., "Modeling canopy conductance and transpiration from solar-induced chlorophyll fluorescence," *Agricultural Forest Meteorol.*, vol. 268, pp. 189–201, 2019.
- [30] N. Shan et al., "A model for estimating transpiration from remotely sensed solar-induced chlorophyll fluorescence," *Remote Sens. Environ.*, vol. 252, 2021, Art. no. 112134.
- [31] Y. Liu et al., "Global assessment of partitioning transpiration from evapotranspiration based on satellite solar-induced chlorophyll fluorescence data," *J. Hydrol.*, vol. 612, 2022, Art. no. 128044.
- [32] K. Zhou et al., "Estimating evapotranspiration using remotely sensed solar-induced fluorescence measurements," *Agricultural Forest Meteorol.*, vol. 314, 2022, Art. no. 108800.
- [33] X. Lu et al., "Potential of solar-induced chlorophyll fluorescence to estimate transpiration in a temperate forest," *Agricultural Forest Meteorol.*, vol. 252, pp. 75–87, 2018.
- [34] B. Pagán et al., "Exploring the potential of satellite solar-induced fluorescence to constrain global transpiration estimates," *Remote Sens.*, vol. 11, 2019, Art. no. 413.
- [35] R. Wang et al., "Scaling solar-induced chlorophyll fluorescence by using VPDO.5 improves the simulation of reference crop evapotranspiration in the arid and semiarid regions of northern China," *J. Hydrol.*, vol. 626, 2023, Art. no. 130254.
- [36] S. Cao et al., "Spatiotemporal dynamics of vegetation net ecosystem productivity and its response to drought in Northwest China," *GIScience Remote Sens.*, vol. 60, no. 1, 2023, Art. no. 2194597.
- [37] H.-J. Xu et al., "Assessing the response of vegetation photosynthesis to meteorological drought across northern China," *Land Degradation Develop.*, vol. 32, no. 1, pp. 20–34, 2020.
- [38] H.-J. Xu, X.-P. Wang, and C.-Y. Zhao, "Drought sensitivity of vegetation photosynthesis along the aridity gradient in northern China," *Int. J. Appl. Earth Observ. Geoinformation*, vol. 102, 2021, Art. no. 102418.
- [39] S. Piao et al., "The impacts of climate extremes on the terrestrial carbon cycle: A review," *Sci. China Earth Sci.*, vol. 49, pp. 1321–1334, 2019.
- [40] M. Li et al., "How has the recent climate change affected the spatiotemporal variation of reference evapotranspiration in a climate transitional zone of Eastern China?," *ISPRS Int. J. Geo-Inf.*, vol. 11, no. 5, 2022, Art. no. 300.
- [41] Y. Zhang et al., "Coupled estimation of 500m and 8-day resolution global evapotranspiration and gross primary production in 2002–2017," *Remote Sens. Environ.*, vol. 222, pp. 165–182, 2019.
- [42] S. Y. He et al., "A daily and 500 m coupled evapotranspiration and gross primary production product across China during 2000–2020," *Earth Syst. Sci. Data*, vol. 14, no. 12, pp. 5463–5488, 2022.
- [43] M. Li, R. Chu, and A. R. M. T. Islam, "A new drought fluorescence monitoring index established for detecting drought evolution characteristics in the middle and lower reaches of the Yangtze River, China during 2001–2020," *IEEE Trans. Geosci. Remote Sens.*, vol. 61, 2023, Art. no. 4405613.
- [44] J. Yang et al., "Estimation of global transpiration from remotely sensed solar-induced chlorophyll fluorescence," *Remote Sens. Environ.*, vol. 303, 2024, Art. no. 113998.
- [45] C. Zheng et al., "Modeling transpiration using solar-induced chlorophyll fluorescence and photochemical reflectance index synergistically in a closed-canopy winter wheat ecosystem," *Remote Sens. Environ.*, vol. 302, 2024, Art. no. 113981.
- [46] W. H. Maes et al., "Sun-induced fluorescence closely linked to ecosystem transpiration as evidenced by satellite data and radiative transfer models," *Remote Sens. Environ.*, vol. 249, 2020, Art. no. 112030.
- [47] K. R. Ahmed et al., "Empirical insights on the use of sun-induced chlorophyll fluorescence to estimate short-term changes in crop transpiration under controlled water limitation," *ISPRS J. Photogrammetry Remote Sens.*, vol. 203, pp. 71–85, 2023.
- [48] W. Yuan et al., "Increased atmospheric vapor pressure deficit reduces global vegetation growth," *Sci. Adv.*, vol. 5, 2019, Art. no. eaax1396.
- [49] S. Zhou et al., "Projected increases in intensity, frequency, and terrestrial carbon costs of compound drought and aridity events," *Sci. Adv.*, vol. 5, 2019, Art. no. eaau5740.
- [50] R. Qiu et al., "Contrasting responses of relationship between solar-induced fluorescence and gross primary production to drought across aridity gradients," *Remote Sens. Environ.*, vol. 302, 2024, Art. no. 113984.
- [51] J. Bai et al., "Estimation of global GPP from GOME-2 and OCO-2 SIF by considering the dynamic variations of GPP-SIF relationship," *Agricultural Forest Meteorol.*, vol. 326, 2022, Art. no. 109180.
- [52] Y. Bai et al., "Variation in ecosystem water use efficiency along a southwest-to-northeast aridity gradient in China," *Ecological Indicators*, vol. 110, 2020, Art. no. 105932.
- [53] C. Frankenberg et al., "New global observations of the terrestrial carbon cycle from GOSAT: Patterns of plant fluorescence with gross primary productivity," *Geophysical Res. Lett.*, vol. 38, 2011, Art. no. L17706.
- [54] N. G. McDowell et al., "Mechanisms of plant survival and mortality during drought: Why do some plants survive while others succumb to drought?," *New Phytologist*, vol. 178, no. 4, pp. 719–739, 2008.
- [55] L. Jiang, B. Liu, and Y. Yuan, "Quantifying vegetation vulnerability to climate variability in China," *Remote Sens.*, vol. 14, 2022, Art. no. 3491.
- [56] J. Chen et al., "Assessment of terrestrial ecosystem sensitivity to climate change in arid, semi-arid, sub-humid, and humid regions using EVI, LAI, and SIF products," *Ecological Indicators*, vol. 158, 2024, Art. no. 111511.
- [57] J. Su et al., "Quantifying the drought sensitivity of grassland under different climate zones in Northwest China," *Sci. Total Environ.*, vol. 910, 2024, Art. no. 168688.
- [58] B. Poulter et al., "Contribution of semi-arid ecosystems to interannual variability of the global carbon cycle," *Nature*, vol. 509, pp. 600–603, 2014.
- [59] Y. Zhan et al., "Spatial differentiation characteristics of vegetation greening rates and climate attribution in China's arid and semi-arid regions," *Glob. Ecol. Conservation*, vol. 46, 2023, Art. no. e02563.
- [60] M. Berdugo et al., "Global ecosystem thresholds driven by aridity," *Science*, vol. 367, pp. 787–790, 2020.
- [61] L. Yang et al., "Evolution of NDVI secular trends and responses to climate change: A perspective from nonlinearity and nonstationarity characteristics," *Remote Sens. Environ.*, vol. 254, 2021, Art. no. 112247.
- [62] A. Damm et al., "On the seasonal relation of sun-induced chlorophyll fluorescence and transpiration in a temperate mixed forest," *Agricultural Forest Meteorol.*, vol. 304, no. 305, 2021, Art. no. 108386.
- [63] Q. Zhang et al., "Solar-induced chlorophyll fluorescence sheds light on global evapotranspiration," *Remote Sens. Environ.*, vol. 305, 2024, Art. no. 114061.
- [64] M. Wang and L. Zhang, "Synchronous changes of GPP and solar-induced chlorophyll fluorescence in a subtropical evergreen coniferous forest," *Plants*, vol. 12, 2023, Art. no. 2224.
- [65] J. Jin et al., "Decoupled driving forces of variabilities of transpiration in Chinese subtropical vegetation based on remote sensing data," *J. Geographical Sci.*, vol. 33, no. 11, pp. 2159–2174, 2023.
- [66] R. Wang and J. Zheng, "The reconstructed solar-induced chlorophyll fluorescence dataset reveals the almost ubiquitous close relationship between vegetation transpiration and solar-induced chlorophyll fluorescence," *J. Hydrol.*, vol. 642, 2024, Art. no. 131883.
- [67] G. Wu et al., "Attributing differences of solar-induced chlorophyll fluorescence (SIF)-gross primary production (GPP) relationships between two C4 crops: Corn and miscanthus," *Agricultural Forest Meteorol.*, vol. 323, 2022, Art. no. 109046.
- [68] Y. Jing et al., "Design and verification of the spectrometer on 'Gou Mang' satellite," *Chin. Space Sci. Technol.*, vol. 43, no. 6, pp. 142–149, 2023.



**Meng Li** received the B.S. degree in biomedical engineering from Shandong University, Jinan, China, in 2011, and the Ph.D. degree in applied meteorology from Nanjing University of Information Science and Technology, Nanjing, China, in 2018.

Since September, 2022, she has been working with the School of Civil Aviation, Zhengzhou University of Aeronautics, Zhengzhou, China. Her research interests include agricultural meteorology, intelligent agriculture, agricultural resources and environment, quantitative remote sensing, and field and regional evapotranspiration.



**Ronghao Chu** received the Ph.D. degree in applied meteorology from Nanjing University of Information Science and Technology, Nanjing, China, in 2019.

Since November 2022, he has been working with Henan Institute of Meteorological Sciences, Zhengzhou, China. His research interests include agricultural meteorology, drought monitoring, quantitative remote sensing, and field and regional evapotranspiration.



**Abu Reza Md. Towfiqul Islam** received the Ph.D. degree in climate change and climate systems from the Nanjing University of Information Science and Technology, Nanjing, China, in 2017.

He has been working as an Associate Professor with the Department of Disaster Management, Begum Rokeya University, Rangpur, Bangladesh. He is acting as Dean of the Faculty of Life and Earth Sciences, Begum Rokeya University. He is an Associate Fellow of the Bangladesh Academy of Sciences (2020), the apex body for scientists in Bangladesh.

He obtained a Postdoctoral Fellowship (2021–2022) from the Prince of Songkla University, Thailand, and the Universiti Teknologi Malaysia (UTM), Malaysia. His major fields of expertise are natural hazards, disaster management, climate change, water quality, flood susceptibility, pollution, human health risk, sediment quality, water resource monitoring, and management. He has authored one book, eight book chapters, more than 250 SCI/SCIE peer-reviewed research papers, participated in ten keynote or participating conferences, and received three awards or recognitions. He is a Review Editor in the *Frontiers in Water* journal, an Associate Editor in *Frontiers in Built Environment and Engineering* and *Frontiers in Public Health*, a Guest Editor in *Frontiers in Climate, Sustainability*, and has also served as a Reviewer for many internationally reputed journals.



**Xiuzhu Sha** received the B.S. degree in applied meteorology from Shenyang Agricultural University, Shenyang, China, in 2012, and the master's degree in applied meteorology from Nanjing University of Information Science and Technology, Nanjing, China, in 2015.

Since July, 2015, she has been working with Weather Modification Center of Henan Province, Zhengzhou, China. Her research interests include atmospheric cloud physics and weather modification.